# TRIUMF

# ANNUAL REPORT
# SCIENTIFIC ACTIVITIES
# 1997

CANADA'S NATIONAL MESON FACILITY
OPERATED AS A JOINT VENTURE BY:

UNIVERSITY OF ALBERTA
SIMON FRASER UNIVERSITY
UNIVERSITY OF VICTORIA
UNIVERSITY OF BRITISH COLUMBIA

UNDER A CONTRIBUTION FROM THE
NATIONAL RESEARCH COUNCIL OF CANADA

ASSOCIATE MEMBERS:

UNIVERSITY OF MANITOBA
UNIVERSITÉ DE MONTRÉAL
UNIVERSITY OF REGINA
UNIVERSITY OF TORONTO

APRIL 1998

*The contributions on individual experiments in this report are outlines intended to demonstrate the extent of scientific activity at TRIUMF during the past year. The outlines are not publications and often contain preliminary results not intended, or not yet ready, for publication. Material from these reports should not be reproduced or quoted without permission from the authors.*

## NUCLEAR AND ATOMIC PHYSICS

### Experiment 560
### Low energy $\pi^{\pm}\vec{p}$ analyzing powers with CHAOS

*(G.R. Smith, K. Raywood, TRIUMF; G. Hofman, UBC)*

This experiment makes use of the CHAOS spectrometer and a specially designed CHAOS polarized proton target (CPPT). The experimental goals of Expt. 560 are to measure the analyzing power ($A_y$) for $\pi^{\pm}p$ scattering to better than $\pm 0.05$ between angles of $\sim 60°$ and $180°$ at several bombarding energies between 30 and 140 MeV. The 1995/1996 beam periods were aimed at resonance energies due to persistent problems with the polarized target. The running period which took place in the fall of 1997, however, enjoyed flawless operation of the target (and spectrometer), and the low energy region was successfully explored with incident $\pi^-$. Unfortunately, the beam time available to this experiment in the fall was insufficient to pursue the $\pi^+$ part of the program, however, that will be dealt with in a forthcoming experiment at PSI.

Using the technique of single energy partial wave analysis (PWA), the data obtained in this experiment will be used to filter out differential cross section ($d\sigma/d\Omega$) measurements which are inconsistent with the $A_y$ data. At present the low energy $d\sigma/d\Omega$ data base contains a number of gross inconsistencies between experiments. In order to determine the $\pi N$ partial wave amplitudes with precision, reliable and precise $d\sigma/d\Omega$ data (which fix the larger amplitudes) must be combined with reliable and precise $A_y$ data (which fix the smaller amplitudes). Analyzing power results in the forward angle (Coulomb-nuclear interference) region for $\pi^+p$ scattering, and in the S-P interference region at backward angles near 50 MeV for $\pi^-p$ scattering are especially useful in this regard. With accurate $\pi N$ partial wave amplitudes, in particular at low energies, the physics goals of Expt. 560 are then to provide improved values for the $\pi N$ coupling constant, to extrapolate to threshold where the $\pi N$ scattering lengths can be obtained, and to extrapolate below threshold as well to obtain a more accurate measure of the $\pi N$ sigma term. The $\pi N$ sigma term is an explicit measure of chiral symmetry breaking from which the strange sea quark content of the proton can be deduced.

The target polarization scheme used for this experiment is complex. The target is polarized in a 2.5 T superconducting solenoid on top of the spectrometer, and lowered down $\sim$1.1 m into the spectrometer while in a frozen spin mode. A small superconducting magnet inside the target cryostat keeps the target polarized during this motion. Once in place, the CHAOS spectrometer field is sufficient to keep the target polarization frozen. Temperatures on the order of 70 mK have been typical during target operation. Polarization losses during the critical transport of the target from the polarizing solenoid to the spectrometer mid-plane are only 2%, typically.

Problems with the polarized proton target have plagued this experiment from the beginning. The situation was summarized in last year's progress report. In 1997 the experiments described there were analyzed, a Ph.D. thesis (Hofman) was obtained based on those data, and the final results are being written up for publication. In this year's progress report, we focus now on the results of the fall, 1997 Expt. 560 running period.

As a result of the many previous problems with the CPPT, the fall effort took place in the M11 channel rather than the (low energy) M13 channel. This was because in M11 the target polarization could be checked by comparison to previous measurements of the analyzing power at resonance energies. This check was performed at the start of the measurement (140 MeV incident $\pi^+$) and verified the target polarization determined by NMR techniques was indeed $\sim$0.82.

As a result, in what turned out to be a very successful run, data were subsequently acquired for incident $\pi^-$ at 51, 57, 67, 87, 98, 117, and 140 MeV. Graphite background data were also collected. The resulting data base spans the S-P interference region which is 'centered' at 57 MeV, 180°. Most of the beam time was devoted to the 57 MeV measurement. There the backward angle cross sections are less than 1$\mu$b/sr, more than 3 orders of magnitude less than the corresponding cross sections at 140 MeV. However, it has been shown that the greatest sensitivity to the scattering lengths is right at the S-P interference minimum, so enough time was spent collecting data in this most difficult region to obtain approximately $\pm 0.08$ uncertainty at the most backward angle, with uncertainities at almost all other angles (and energies) typically $\pm 0.02$ or less.

In order to obtain data in to the smallest possible scattering angles at the lowest three energies in particular, the CHAOS first level trigger (1LT) was programmed for 'singles' mode so that any scattered pion could generate a 1LT. This would have led to an impossible situation due to the overwhelming background of quasielastic $\pi^-n$ scattering (the polarized target consists of butanol, $C_4H_9OH$) were it not for innovative changes which were made to the second level trigger (2LT). The 2LT was programmed to recognize 'short tracks', i.e. protons which were observed in the correct angular region and with the expected curvature based exclusively on information from only the inner

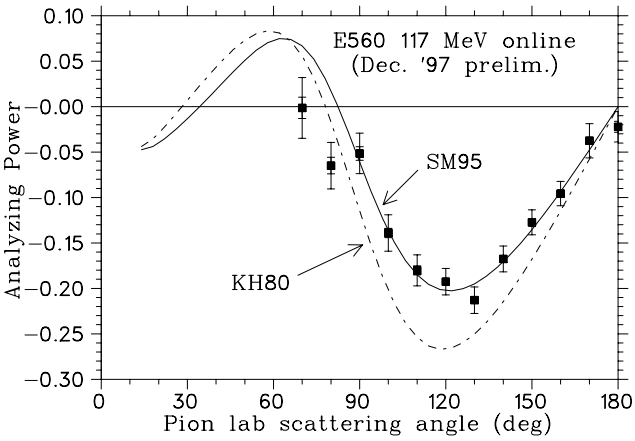


Fig. 23. Preliminary on-line angular distribution of the $\pi^- p$ analyzing power measured with CHAOS in the fall of 1997 at 117 MeV. Also shown are the results of two partial wave analyses: SM95 (solid line) and KH80 (dashed line).

two wire chambers. Events with (recoil) protons whose trajectories stopped outside of WC2 were not lost; if the protons failed to make it to WC3 their trajectories were determined by combining the pion vertex with the proton hits registered in WC1/2. Events with protons which made it at least to WC2 were required in the (second level) trigger, which reduced trigger rates to manageable levels (typical live times were ∼90–95%) without having to resort to a doubles 1LT with its corresponding abbreviation of the measured angular distribution.

An example of preliminary analyzing powers obtained in the fall running period is shown in Fig. 23 for the case of 117 MeV incident $\pi^-$. These are on-line results. Two error bars are plotted, one based on the on-line statistics, the other based on what the error is projected to be after recovering the full statistics available in off-line replay. For most points, this latter error is smaller than the plotted point (smaller than $\pm 0.01$) and is thus not visible. The on-line data are acquired with very loose software requirements so it is usual that after more careful analysis the points can move, in particular the forward angle points where the background requires more careful treatment than that given on-line. Having said this, however, the agreement of these preliminary, on-line results with the partial wave solution SM95 is remarkable.

**Experiment 561**
**Determination of the $\pi^\pm p \to \pi^\pm \pi^+ n$ cross section near threshold**
*(M.E. Sevior, Melbourne)*

Though widely successful in particle physics, QCD is notoriously difficult to apply at low energies. However, with the development of chiral perturbation theory (ChPT) which exploits the chiral symmetries of QCD [Gasser and Sevior, Proc. Workshop on Chiral Dynamics (1994) 107], a means is now available for addressing low energy questions such as the determination of the strength of the simplest of the strongly interacting systems, the $\pi - \pi$ interaction. One of the most fruitful ways of investigating this interaction experimentally has involved the measurement of threshold pion-induced pion production cross sections. Bernard *et al.* [Int. J. Mod. Phys **E4**, 193 (1995); Nucl. Phys. **B457**, 147 (1995); Nucl. Phys. **A619**, 261 (1997)] have shown that the amplitudes at threshold for pion induced pion production can be related through chiral perturbation theory to the underlying $\pi - \pi$ scattering lengths.

Given the importance of a precise determination of the $\pi - \pi$ scattering lengths, Expt. 561 performed near threshold cross section measurements of both $\pi^+ p \to \pi^+ \pi^+ n$ and $\pi^- p \to \pi^- \pi^+ n$.

The data-taking was completed in 1991. The final analysis was completed this year.

The experiment was performed at TRIUMF on the M11 beam line at 200, 190, 184, 180 and 172 MeV for the negative pions and at 200, 184 and 172 MeV for the positive. In each case, the data obtained at 172 MeV provided background information, since this energy is below the threshold for the reactions of interest (172.3 MeV).

The apparatus consisted of a beam tracking system of 3 scintillators, a 5 segment active target of 6 mm thick PILOT-U scintillators ($C_1H_{1.1}$), an array of 14 "neutron" bar scintillators placed 3 m downstream of the target and a deflecting magnet to sweep charged particles away from the neutron bars. Such an arrangement minimized the effects of the substantial $\pi^+$ C $\to \pi^+ nX$ background by exploiting the kinematics of the near-threshold reaction of interest, particularly the restriction of the neutrons to a narrow forward cone.

Positive pions produced (and stopped) in the target were identifed by their signature decay, $\pi^+ \to \mu^+ \nu_\mu$, using three different techniques to identify and measure the height and relative time of occurrence of the pulses following the initial pion pulse in any target segment [Raywood *et al.*, Nucl. Inst. and Methods **A365**, 135 (1995)]. One of these techniques included the use of TRIUMF 500 MHz transient digitizers attached to the target scintillation counters.

The experimental yields were evaluated from peak areas in histograms of $T_{\rm sum}$, the sum of the kinematic energies of the reaction products, $T_n + \Sigma T_\pi$, which is constant for the $\pi p \to \pi\pi n$ reaction but produces a continuum for the background. The neutron kinetic energy, $T_n$, was determined from the time of flight from the active target to the detection array whereas the

kinetic energy of the produced pions, $\Sigma T_\pi$, was taken as the total energy deposited in the active target.

$T_{\rm sum}$ spectra were generated by two different techniques for the $\pi^+$ channel. The first ("one $\pi$" method) required only the coincident detection of a neutron with a single stopping $\pi^+$ (and its subsequent decay) in the target. In this method, the substantial $\pi^+$ C $\rightarrow \pi^+ nX$ background was suppressed by restricting the allowed kinematic ranges for the $T_\pi$ and $T_n$ spectra. These ranges were determined from the logical AND of the ranges allowed by the kinematics of the $\pi^+ p \rightarrow \pi^+\pi^+ n$ reaction with the observed ranges. The remaining background was determined by subjecting the data at 172 MeV to the same kinematic restrictions as the $T_{\rm sum}$ spectra under study.

The second technique employed to extract yields ("two $\pi$" method) required the detection of two positive pions in the target, each in a different target segment. The requirement of detecting a second $\pi^+$ substantially reduced the background. The backgrounds for this "two $\pi$" analysis were determined in similar fashion to those for the "one $\pi$" analysis. For each of the two methods, the experimental acceptances needed to enable determination of the cross sections from the measured yields were determined by Monte Carlo simulations. The results are summarized in Table I.

For the $\pi^-$ channel, only one positive pion was present in the final state. Thus, only the first ("one $\pi$") method of analysis could be employed. Stopped negative pions are rapidly absorbed by carbon nuclei when stopped. Although the nuclei eject energetic fragments when the pions are absorbed, about 50% of the time only neutral particles are emitted. When this occurs the $\pi^- p \rightarrow \pi^+\pi^- n$ event falls in a well defined $T_{sum}$ peak. Such behaviour for stopping negative pions was confirmed in calibration runs when the pions from M11 were stopped in each segment of the active target in turn. The resultant pulse height distributions were used in the Monte Carlo code employed to simulate the experiment.

This experiment provides cross section data for *both* $\pi^+$ and $\pi^-$ incident beams and provides the only data which extend to within 8 MeV of threshold.

Table I. Total cross sections for $\pi^\pm p \rightarrow \pi^\pm\pi^+ n$. The listed uncertainties include both statistical and systematic errors.

| | Cross sections ($\mu b$) | |
|---|---|---|
| $T_\pi$ | $\pi^+ p \rightarrow \pi^+\pi^+ n$ | $\pi^- p \rightarrow \pi^-\pi^+ n$ |
| (MeV) | Averaged | One $\pi$ |
| 200 | $1.4 \pm 0.3$ | $6.5 \pm 0.9$ |
| 190 | – | $3.0 \pm 0.5$ |
| 184 | $.30 \pm .07$ | $1.9 \pm 0.3$ |
| 180 | – | $0.7 \pm 0.1$ |

Although the $\pi^-$ data agree with the OMICRON results (as well as with other data sets) at the higher energies, the $\pi^+$ data agree with the results of Sevior rather than with OMICRON. Using the formulation of Bernard *et al.* [*op. cit.*], our cross section data yield threshold values for the matrix elements: $|\mathcal{A}_{10}| = (8.5\pm0.6)m_\pi^{-3}$ and $|\mathcal{A}_{32}| = (2.5\pm0.1)m_\pi^{-3}$, and for the $\pi-\pi$ scattering lengths: $a_0 = (0.23\pm0.08)m_\pi^{-1}$, and $a_2 = (-0.031\pm0.008)m_\pi^{-1}$. Our value for $|\mathcal{A}_{10}|$ is in good agreement with the value of $8.0\pm0.3m_\pi^{-3}$ obtained by Bernard *et al.* [*op. cit.*] from an analysis of the $\pi^- p \rightarrow \pi^0\pi^0$ data of Lowe *et al.* [Phys. Rev. Lett. **C44**, 956 (1991)] and our values of the scattering lengths are in agreement within errors with the chiral perturbation theory predictions of Gasser and Leutwyler [Phys. Lett. **125B**, 321 (1983); **125B**, 325 (1983)]: $a_0 = (0.20 \pm 0.1)m_\pi^{-1}$ and $a_2 = (-0.042 \pm 0.02)m_\pi^{-1}$. The uncertainties in our experimental values of the scattering lengths are dominated by the theoretical uncertainties as estimated by Bernard *et al.* [*op. cit.*].

**Experiment 591**
**The role of 3NA in $^{12}$C($\pi^+, ppp$) and $^{12}$C($\pi^+, ppn$) reactions**
*(R. Tacik, TRIUMF/Regina)*

This experiment received beam time in 1992, but is currently being re-analyzed in light of the new results on pion absorption obtained with the CHAOS detector (Expt. 722). This analysis constitutes the M.Sc. thesis project of Mr. P. Barghava of the Univ. of Regina.

Experiment 591 was run in the M11 channel, employing pions with incident kinetic energies of 100, 165, and 235 MeV. A thin slab of plastic scintillator was used as an active carbon target. There were four detectors for outgoing nucleons. Three of these were stopping counters, and the fourth was a time-of-flight (TOF) array. The stopping counters consisted of a large segmented block of plastic scintillator (approx. $20 \times 20 \times 30$ cm$^3$), preceded by thin plastic $\Delta E$ counters and two wire chambers. The TOF array consisted of two layers of plastic scintillator bars. Each layer was composed of ten vertically mounted bars with volume $10 \times 10 \times 100$ cm$^3$. The front face of the array was positioned 200 cm from the target centre. It was preceded by thin plastic veto counters. The experimental trigger required a coincidence of any three of the four detectors. The information from the TOF veto counters was recorded, but not included in the hardware trigger. Thus, the array was used to detect both protons and neutrons.

Data were taken at several angular settings of the stopping counters. At each setting, the position of the TOF array was varied to provide a wide angular coverage. Some typical angular distributions, measured at

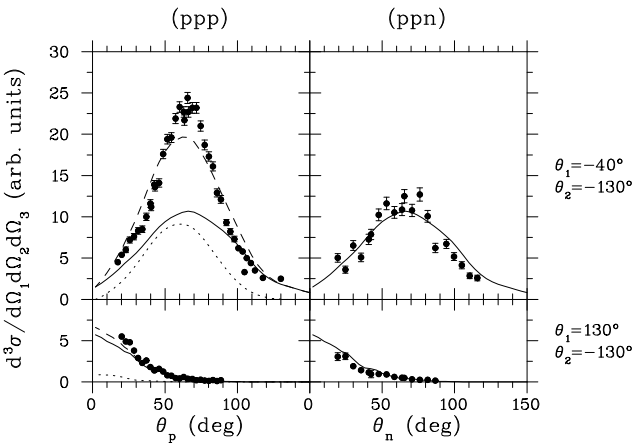


Fig. 24. Angular distributions measured in Expt. 591. See text for an explanation of the various curves.

$T_\pi$ = 165 MeV, are shown in Fig. 24. The solid lines in this figure represent the results of a model calculation in which the pion absorption occurs on four nucleons, resulting in a *pppn* final state. This model provides a reasonable description of the (*ppn*) data, but predicts a much broader angular distribution than is actually measured for the (*ppp*) data, at certain angular settings. The dotted lines in Fig. 24 represent the simulated contributions of the two-step process of $\pi^+p$ quasielastic scattering followed by two-nucleon absorption. This process was identified as contributing to the CHAOS (*ppp*) data. Such a two-step process would be expected to have a smaller impact on (*ppn*) final states, because it would have to involve $\pi^+n$ quasielastic scattering in the first step. The dashed curves in Fig. 24 show the sum of the solid and dashed lines, and provide an improved description of the measured (*ppp*) distributions.

**Experiment 613**
**Reactions of muonic hydrogen isotopes**
*(G.M. Marshall, TRIUMF)*

Two limitations exist to the number of fusion interactions which can be catalyzed by one muon in a mixture of tritium and deuterium. The first is the rate $\lambda_{dt\mu}$ at which a muonic molecular ion ($dt\mu$) is formed, and the second is the probability $\omega_s$ that the muon will stick to the alpha particle following fusion, ending the series of fusions in the catalysis cycle. Experiment 613 is designed to provide a direct experimental measurement of $\lambda_{dt\mu}$, which is dominated by a resonance mechanism in which the kinetic energy of the projectile (muonic tritium, $t\mu$) is absorbed in the internal molecular degrees of freedom of an excited muonic molecular complex ($[(dt\mu)^+dee]^*$, for a target of $D_2$, or $[(dt\mu)^+pee]^*$, for $HD$). The most interesting energy range, where the rate is highest, is between 0.1 and 2.0 eV and is well beyond the thermal range of typical hydrogen targets.

Theoretical predictions exist for the resonant energy dependence of the rate in this range, for target molecules of $D_2$ and $HD$. In Expt. 613, the time-of-flight method and two thin separated layers of solid hydrogen isotope mixtures have been used to measure a distribution which is quite sensitive to the rate. A production layer is composed of a mixture of protium ($^1H_2$) with 0.1% tritium. Muons form muonic protium and then rapidly transfer to tritons, forming $t\mu$ atoms with energies up to 40 eV as a result of the energy released in the transfer process. Because the interaction of $t\mu$ with protons is small, the fast muonic atoms are emitted from the thin layer. The energy is moderated to the range of interest with an overlayer of $D_2$, and the muonic atoms travel approximately 2 cm before reaching a separate reaction layer of $D_2$ or $HD$, where fusion occurs with a rate depending on the energy. The time distribution between the muon stopping in the production layer, and the fusion in the reaction layer, reflects the energy structure of the rate.

Because the time distribution is related in a complex way to the resonant energy structure, a computer simulation of all relevant processes has been developed to understand the data. It is necessary to include many energy-dependent reactions such as muonic atom formation, scattering (including angular dependence), muon transfer, and non-resonant molecular formation. Fortunately, sophisticated calculations exist in

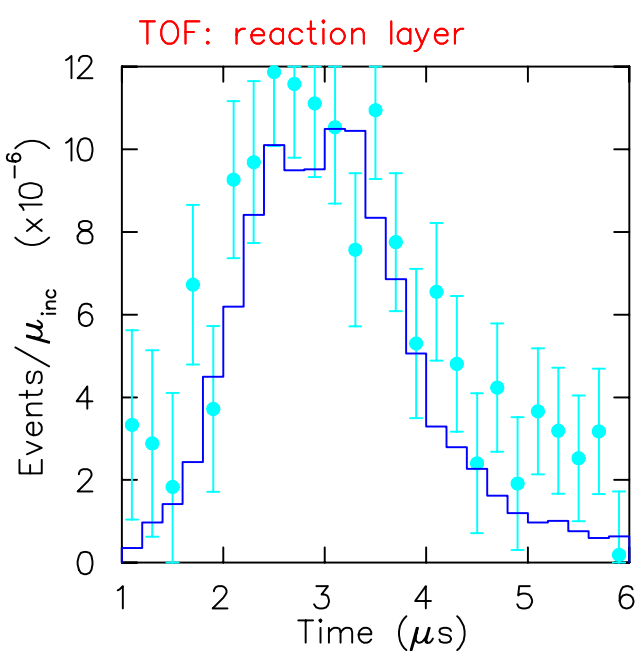


Fig. 25. Experimental time of flight distribution (filled circles) compared with results of simulation (histogram). The results are preliminary.

all cases. Significant progress was made in the past year to improve the quality and detail of the simulation, testing it with comparisons to data taken in the past under different conditions which emphasize different important processes. In some cases, the theoretical predictions seem to be supported, but in others there exist significant discrepancies. In particular, there is approximate agreement of the simulation based on theoretical resonant molecular formation rates with time-of-flight data for $t\mu$ on thin $D_2$ reaction layers (Fig. 25). With somewhat thicker layers, the agreement is not as good, perhaps indicating an inadequate muonic atom thermalization model.

Data from reaction layers of both $D_2$ and $HD$ are currently being analyzed for two doctoral theses.

**Experiment 624**

**The $(\pi, 2\pi)$ reaction, a tool to determine scattering lengths and coupling constants**

*(G.R. Smith, TRIUMF; M. Kermani, UBC)*

This experiment received beam time during the high intensity periods of TRIUMF operation between January and August, 1994. A liquid hydrogen target was employed with the CHAOS spectrometer in the TRIUMF M11 beam line.

The experiment focused on a systematic investigation of the $H(\pi^{\pm}, 2\pi)$ reaction in a series of exclusive measurements. For incident $\pi^-$, the $H(\pi^-, \pi^+\pi^-)n$ and the $H(\pi^-, \pi^-\pi^0)p$ channels were measured simultaneously by detecting the two charged particles in the final state in coincidence. Likewise for incident $\pi^+$, the $H(\pi^+, \pi^+\pi^+)n$ and the $H(\pi^+, \pi^+\pi^0)p$ channels were measured simultaneously. Pion bombarding energies of 220, 240, 260, 280, and 300 MeV were studied and approximately 10,000 $(\pi, 2\pi)$ events were recorded at each energy for the channels with two charged pions in the final state. In addition, $\pi p$ elastic data were acquired at each energy and pion polarity in order to provide checks on the absolute normalization.

The analysis of the $H(\pi^{\pm}, \pi^+\pi^{\pm})n$ data is complete. The data at each of the energies have been analyzed and the necessary acceptance calculations, which involve detailed Monte Carlo simulations of the reaction folding in the detector acceptance, have been finished. Some aspects of the experimental results have been described in previous Annual Reports: examples of the missing mass spectrum obtained with CHAOS and with the detector simulation package, as well as particle identification results. Most of our effort since then has focused on interpreting the results and finishing the $\pi^+\pi^+$ data analysis. That has been accomplished. The Ph.D. thesis (Kermani) associated with this work has also been finished. Our remaining effort on Expt. 624 is just to write up for publication the analyses we have already done.

The $(\pi, 2\pi)$ reaction at a given energy can be completely described in terms of four variables: the dipion invariant mass squared ($m^2_{\pi\pi}$), the four-momentum transfer to the nucleon squared (t), the angle between the two $\pi^-$ in the dipion rest frame ($\theta$), and an out-of-plane angle ($\psi$). The first three of these variables are well covered by the CHAOS acceptance. Although only about 10% of the latter variable is covered, the out-of-plane departures from phase space are small in the energy regime covered by this experiment [Ortner *et al.*, Phys. Rev. **C47**, 447 (1993)]. In fact, the total cross sections obtained at each of the five energies studied agree well with previously published results obtained mostly with ($4\pi$ sr) bubble chambers.

The results of the experiment were loaded into a three dimensional lattice consisting of ten bins in each of $m^2_{\pi\pi}$, t, and $\cos(\theta)$, with each node in the lattice weighted according to the acceptance determined from the simulations. The $\cos(\theta)$ dependence was integrated out, yielding double differential cross sections $d^2\sigma/dm^2_{\pi\pi}dt$. Single and total cross sections were obtained by successive integration.

The Chew-Low formalism is a model-independent technique for isolating the one-pion-exchange (OPE) diagram of interest by extrapolating the 2-fold differential cross sections to the (unphysical) pion pole at t=+1 (in units of $m^2_{\pi}$). The physical threshold is at t=0. Since the CHAOS data fall primarily into the near threshold, small $m^2_{\pi\pi}$, small t region needed for an accurate extrapolation, our results are well suited for this type of analysis. Although the Chew-Low method is model-independent, it does assume OPE dominance in the extrapolation region. Unfortunately, it appears that for the $H(\pi^+, \pi^+\pi^+)n$ results, the influence of the $\Delta$ diagrams renders the extrapolation unreliable. However, the $H(\pi^-, \pi^+\pi^-)n$ Chew-Low analysis was successful. For this reaction channel several arguments necessary for (but not sufficient to prove) OPE dominance can be made. The results of this analysis were submitted to Physical Review Letters in December, 1996. In last year's Annual Report we showed the on-shell $\pi\pi$ cross sections obtained as a function of $m^2_{\pi\pi}$ derived from the Chew-Low analysis of the CHAOS data. This results in the most precise measure to date of $a^0_0$. We obtain $a^0_0 = 0.209 \pm 0.032$ in units of the inverse pion mass. The best previous experimental value for $a^0_0$ (determined from $K_{e4}$ decay) is $0.28 \pm 0.05$ [Rosselet *et al.*, Phys. Rev. **D15**, 574 (1976)].

An extended model [Sossi *et al.*, Nucl. Phys. **A548**, 562 (1992)] of Oset and Vicente-Vacas has also been applied to the experimental results. Besides providing values for several $\Delta$ and $N^*$ coupling constants, this (model-dependent) approach can be used to provide the chiral perturbation theory parameters $L_1$ and $L_2$.

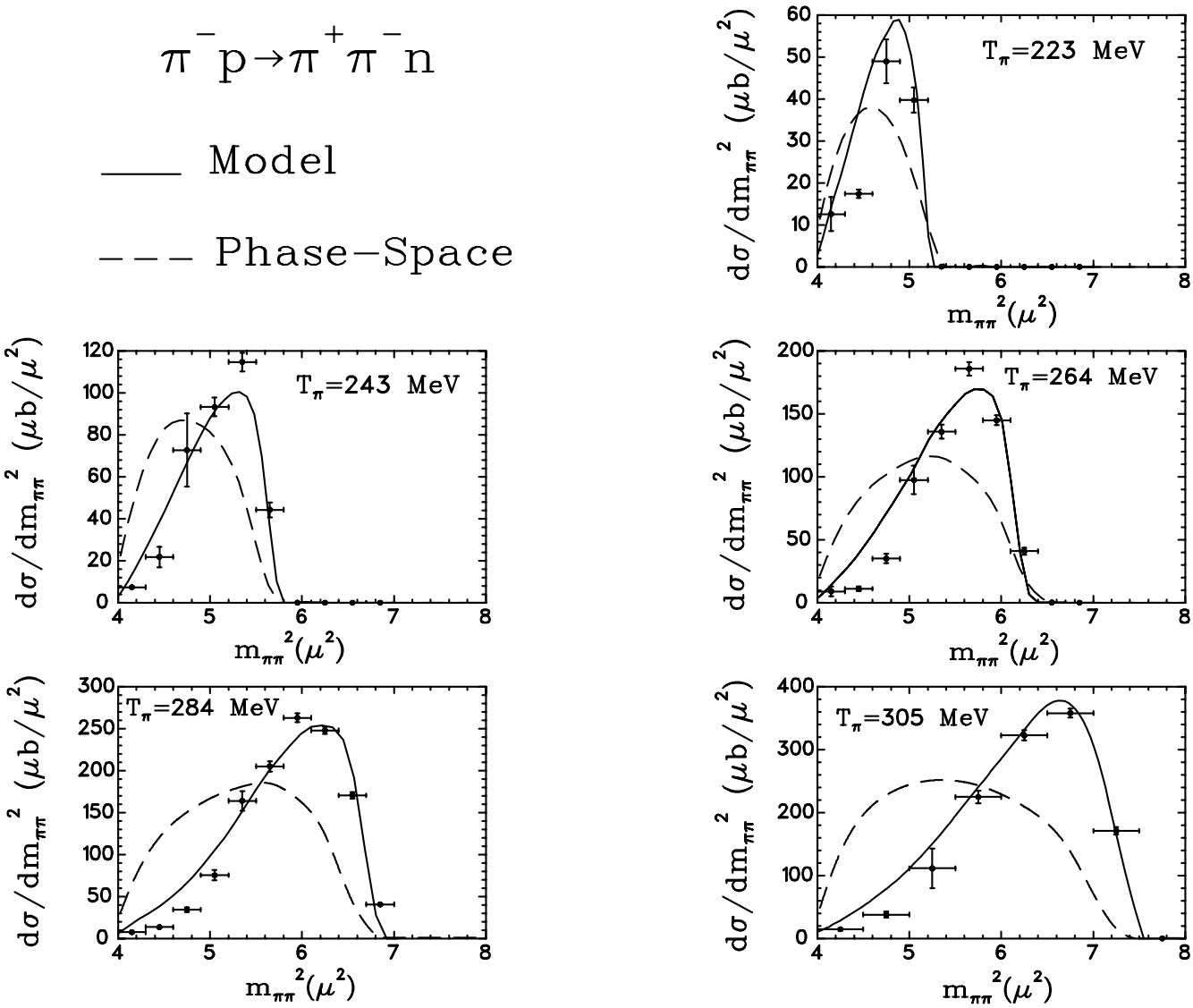


Fig. 26. The $m^2_{\pi\pi}$ distributions in the $H(\pi^-, \pi^+\pi^-)n$ channel are shown along with the corresponding phase space curves (dashed) and fits obtained with the model (solid lines) at each of the energies measured in the experiment.

The fits to the measured $m^2_{\pi\pi}$ distributions in the $H(\pi^-, \pi^+\pi^-)n$ channel obtained using the model are shown in Fig. 26 along with the corresponding phase space curves.

**Experiment 633**
**A measurement of $pp \to pn\pi^+$ at 420 and 500 MeV**
*(W.R. Falk, Manitoba)*

Inclusive measurements of the pion differential cross sections and analyzing powers have been measured for this reaction over the angular range of 23° to 100° (lab). The pion energy range extended from the three-body upper limit down to pion energies as low as 20 MeV, representing internal *np* excitation energies as high as 80 MeV. Experimental details and some preliminary results for this reaction were presented last year. While the 2-body reaction $pp \to d\pi^+$ has been investigated in great detail, only few data previously existed in this energy range for this important $NN \to NN\pi$ reaction. These data fill an important gap between the near-threshold measurements [Daehnick *et al.*, Phys. Rev. Lett. **74**, 2913 (1995); Phys. Rev. C **56**, 20 (1997)] and those measurements above 600 MeV [Hancock *et al.*, Phys. Rev. **C27**, 2742 (1983); Bhatia *et al.*, Phys. Rev. **C28**, 2071 (1983), and references therein]. Some previous inclusive TRIUMF measurements [Falk *et al.*, Phys. Rev. **C32**, 1972 (1985)] fall in the energy range of the present experiment.

The presence of muons, from the decay of pions, formed a significant background for a number of the runs. In many cases these muons could not easily be

separated from the pions because their time of flight and energy loss were almost identical. Fortunately, for some runs a complete separation could be made, and from this information, together with Monte Carlo simulations of the expected muon background, an effective separation could be made.

Distributions of the differential cross sections at 500 MeV are shown in Fig. 27. The data are for the angles (top to bottom) of 23.6, 35.0, 45.0, 55.0, 65.1, 75.2, 85.1 and 100.0 degrees (lab). These data have been multiplied, respectively, by $10^7$, $10^6$, ..., $10^0$. Thus the top curve for 23.6° has a maximum cross section of $\approx 15$ $\mu b/sr$ MeV/c.

The solid curves in this figure represent a simultaneous fit to the data for all the angles (excluding 100°), using model momentum and angular distribution forms in the c.m. frame, as given by Rosenfeld [Phys. Rev. **96**, 139 (1954)] and Gell-Mann and Watson [Ann. Rev. Nuc. Sci. **4**, 219 (1954)]. These model distributions are classified according to the final state partial waves, for example, $Sp$; here the first letter $S$ signifies $\ell_{NN} = 0$ and the second, $p$, signifies $\ell_\pi = 1$. Indeed, at 500 MeV, $Sp$ accounts for about 1740 $\mu b$ of the total cross section of 2780 $\mu b$. This is the dominant partial wave in the $pp \to d\pi^+$ reaction. The partial wave $Ss$ contributes about 170 $\mu b$. A significant contribution to the three-

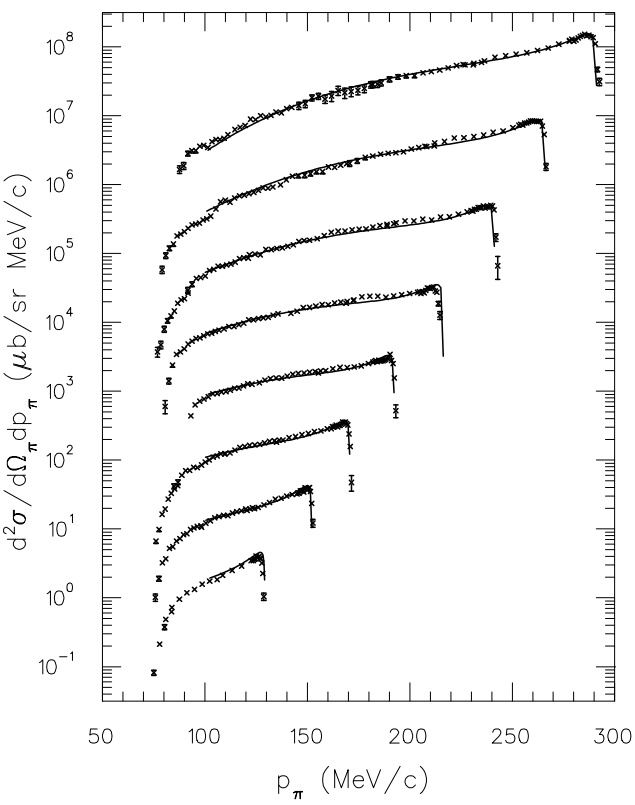


Fig. 27. Differential cross section distributions for the $pp \to pn\pi^+$ reaction at 500 MeV. All quantities are given in the laboratory frame.

body reaction comes from the $Pp$ partial wave (which doesn't contribute to the two-body case), amounting to 360 $\mu b$. Significant also (500 $\mu b$) is the contribution of the $np$ $T = 1$ final state. This was modelled from the $pp \to pp\pi^\circ$ reaction [Stanislaus *et al.*, Phys. Rev. **C44**, 2287 (1991)]. Theoretical comparisons of these differential cross sections will be made with a one boson exchange model [Engel *et al.*, Nuc. Phys. **A 603**, 387 (1996)].

**Experiment 700**
**Measuring cross sections of long-lived radionuclides produced by 200–500 MeV protons in elements found in lunar rocks and meteorites**
*(J. Sisterson, Harvard)*

Small quantities of radionuclides and stable isotopes are produced in lunar rocks and meteorites by cosmic ray interactions. Interpreting this cosmic ray record gives information about the average solar proton flux over the past million years and the history of the irradiated object. Interactions of both solar and galactic cosmic rays (SCR and GCR) contribute to the cosmogenic nuclide archive. The cosmogenic nuclides produced include the radionuclides, $^{10}$Be, $^{14}$C, $^{22}$Na, $^{26}$Al, $^{36}$Cl, the stable neon isotopes $^{20}$Ne, $^{21}$Ne, $^{22}$Ne, and isotopes of Kr. Important elements found in lunar rocks and meteorites include oxygen, silicon, aluminum, magnesium, iron, titanium, potassium, nickel, rubidium, strontium and yttrium.

SCR are ~98% protons with energies usually $\leq 200$ MeV; the solar proton flux is variable and at times of a solar proton event (SPE) can be very high, with event integrated fluxes of $\sim 10^{10}$ p/cm$^2$ (Ep $\geq 10$ MeV) lasting over several days. Such an SPE is a hazard to both humans and equipment if encountered during a space mission. GCR are ~87% protons and can have very high energies and penetrate deeply into the irradiated object.

The theoretical models used to analyze the measured activity-depth profiles of cosmogenic nuclides demand good cross section information as input. Proton production cross sections are extremely important, because so many cosmic ray particles are protons. The cross section measurements made at TRIUMF are essential to extend our knowledge of the excitation functions up to the energy region of the GCR.

The cross section measurements made at TRIUMF are part of an overall program – funded in part by NASA – to measure all of the needed cross sections. The irradiations are made at the proton accelerators at the Univ. of California, Davis, ~20 – ~68 MeV; the Harvard Cyclotron Laboratory (HCL), 40–160 MeV; and TRIUMF, 200–500 MeV. After irradiation, short lived activities for example, $^7$Be, $^{22}$Na and $^{24}$Na, are measured using non-destructive gamma-ray

spectroscopy at TRIUMF and HCL. The targets are then sent to the appropriate collaborators for any necessary chemical preparation and measurement of the cosmogenic nuclide using accelerator mass spectrometry (AMS) or mass spectroscopy (MS). The collaborators include the Univ. of Arizona for $^{14}$C determination by AMS; Lawrence Livermore National Laboratory (LLNL) and San Jose State Univ. for $^{10}$Be, and $^{26}$Al by AMS; LLNL and the Univ. of California, Berkeley for $^{36}$Cl by AMS; LLNL for $^{20}$Ne, $^{21}$Ne and $^{22}$Ne by MS; Kr, Ar and Ne isotopes by MS at the Centre d'Etudes Nucléaires de Bordeaux-Gradignan, France; after the cross sections are measured, theoretical model calculations are made at Los Alamos National Laboratory.

In August, irradiations were made at TRIUMF to produce Kr isotopes in targets of $RbMnF_3$ (for Rb), $SrF_2$ (for Sr) and Y; $^{36}$Cl in $KNO_3$ (for K) and Ti; $^{14}$C in Ti. Short lived activities have been measured in these targets. When neon isotopes are to be measured in a target, it is important to measure the $^{22}$Na produced in the target to correct for the $^{22}$Ne produced from the decay of $^{22}$Na. $^{22}$Na produced in the Rb, Sr and Y targets has been measured, and these targets will be sent for MS determination after the residual activity in the targets has reached acceptable levels. $^{14}$C in the Ti targets will be measured in January, 1998.

In 1997, the results of the following cross section measurements Si$(p,x)^7$Be, Si$(p,x)^{10}$Be, Si$(p,x)^{22}$Na, Si$(p,x)^{26}$Al, O$(p,x)^7$Be and O$(p,x)^{10}$Be [Sisterson *et al.*, Nucl. Instrum. Methods **B123**, 324 (1997)]; Al$(p,x)^7$Be, Al$(p,x)^{10}$Be, Al$(p,x)^{22}$Na, Al$(p,x)^{26}$Al, Mg$(p,x)^7$Be, Mg$(p,x)^{10}$Be, Mg$(p,x)^{22}$Na, and Mg$(p,x)^{26}$Al [Sisterson *et al.*, CP392, Application of Accelerators in Research and Industry, eds. Duggan and Morgan (AIP, New York, 1997) p.811] for $E_p$ 25–500 MeV were published. Revised values for the cross sections O$(p,x)^{14}$C, Si$(p,x)^{14}$C and new measurements of Al$(p,x)^{14}$C, Mg$(p,x)^{14}$C, Fe$(p,x)^{14}$C and Ni$(p,x)^{14}$C for $E_p$ 25–500 MeV are submitted for publication in Geochim. et Cosmochim. Acta (November, 1997). These results, plus those of the European collaboration [Bodemann *et al.*, Nucl. Instrum. Methods **B321**, 9 (1993); Michel *et al.*, Nucl. Instrum. Methods **B103**, 183 (1995); Schiekel *et al.*, Nucl. Instrum. Methods **B114**, 91 (1996)] now allow most of these cross sections to be used with confidence in model calculations. Revised estimates for the production for $^{22}$Na in lunar rock 74275 [Sisterson and Reedy, Lunar Planet. Sci. **XXVII**, 1325 (1997)], and $^{10}$Be and $^{26}$Al production in lunar rock 68815 [Sisterson *et al.*, Lunar Planet. Sci. **XXVII**, 1327 (1997)] using the new cross sections, were presented at the 28th Lunar and Planetary Science meeting in March.

Currently, neon isotopes are being measured using MS at LLNL in Si, Al, Mg and Fe targets. These targets were irradiated at TRIUMF in February, 1996. $^{20}$Ne, $^{21}$Ne, $^{22}$Ne and ($^{22}$Ne + $^{22}$Na) were measured in Al targets in November, 1997 and preliminary results for some Mg and Si targets measured in December, 1997 are available. The cross sections measured at 200, 300, 400 and 500 MeV from the TRIUMF irradiations are the first measured in these elements at these energies. These results will be presented at the 29th Annual Lunar and Planetary Science meeting in March, 1998. Further irradiations at lower energies at HCL and Davis will lead to much better knowledge of these important excitation functions.

**Experiment 704**
**Charge symmetry breaking in $np \rightarrow d\pi^0$ close to threshold**
*(A.K. Opper, Ohio; E. Korkmaz, UNBC)*

Experiment 704, a high precision measurement of charge symmetry breaking (CSB) in the strong interaction, is now fully in "production mode" and as such, continues TRIUMF's contribution to this area of physics. Previous measurements of CSB in $N-N$ scattering have been the precise determination of the difference in analyzing power for elastic *np* scattering, $\Delta A_y$, at TRIUMF [Abegg *et al.*, Phys. Rev. Lett. **56**, 2571 (1986); Phys. Rev. **D39**, 2464 (1989); Abegg *et al.*, Phys. Rev. Lett. **75**, 1711 (1995)] and IUCF [Vigdor *et al.*, Phys. Rev. **C46**, 410 (1992)]. While CSB can be understood as different manifestations of the mass difference between the up and down quarks and electromagnetic effects, the calculations based on meson exchange models best describe these data.

Experiment 704 is an experiment to measure the forward-backward asymmetry ($A_{fb}$) in $np \rightarrow d\pi^0$, which must be zero in the centre of mass if charge symmetry is conserved. Calculations by Niskanen [private communication] give an angle integrated value of approximately $-50 \times (10)^{-4}$ for $A_{fb}$ near 280 MeV with the dominant contributions being an order of magnitude larger than those of the elastic scattering CSB measurements. These contributions are due to the exchange of an isovector-isoscalar mixed meson ($\pi^0 - \eta$) and ($\pi^0 - \eta'$), and differences in $\pi^0 - p$ and $\pi^0 - n$ coupling. As a measure of *inelastic np* scattering, Expt. 704 complements the existing data in that it has contributions which don't exist in elastic *np* scattering.

The experiment is carried out with a 279.5 MeV neutron beam, a liquid hydrogen target, and the SASP spectrometer positioned at 0°. With these kinematics and the large acceptance of SASP the full deuteron distribution can be detected in one setting of the spectrometer thereby eliminating many systematic uncertainties. This experiment requires a measurement of

the $pp \to d\pi^+$ distribution as a test case to verify the analysis and simulation codes, since the deuteron distribution from $pp \to d\pi^+$ must be symmetric in the centre of mass due to the indistinguishability of the two protons.

The $np \to d\pi^0$ and $pp \to d\pi^+$ reactions have been studied near threshold with the MRS in TRIUMF experiments 466 [Hutcheon *et al.*, Nucl. Phys. **A535**, 618 (1991)] and 552 [Korkmaz *et al.*, Nucl. Phys. **A535**, 637 (1991)], respectively. With the factor of four increase in acceptance of SASP over the MRS and what we currently understand about the physical and optical acceptance of SASP, we intend to measure $A_{fb}$ with an overall precision (statistical and systematic) of approximately $\pm 12 \times (10)^{-4}$.

Our activities in 1997 fall into three catagories: finalizing the experimental running conditions, acquiring and analyzing data, and investigating our sensitivity to systematic effects.

**Description of the experiment**

For the most part, the $np \to d\pi^0$ phase of this experiment is carried out with the CHARGEX facility in its standard mode of operation. A schematic of the experimental layout is shown in Fig. 28. A primary proton beam of 500 nA is incident on a thin neutron-production $^7$Li target. A clearing magnet, the CHARGEX dipole, will sweep unscattered protons into a well-shielded beam dump, 4B3.

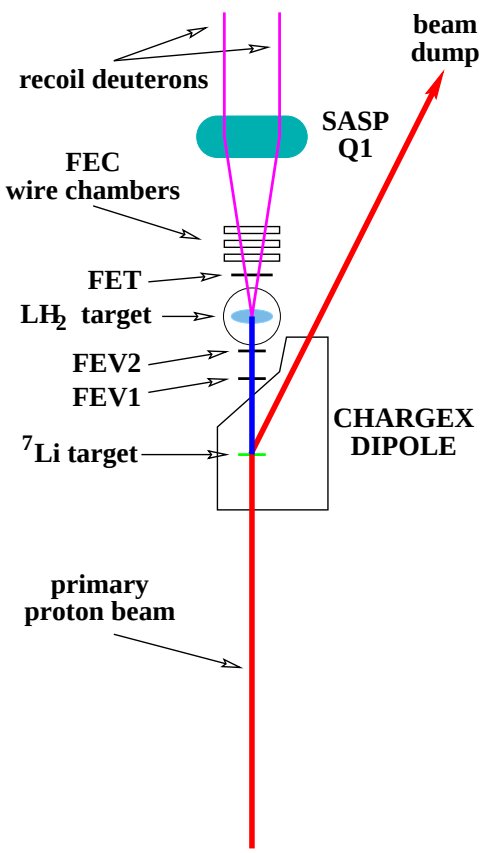


Fig. 28. Schematic drawing of CHARGEX neutron-beam facility, $LH_2$ target, and front end detectors for $np \to d\pi^0$ measurement.

After passing through two sets of segmented veto scintillators (FEV1 and FEV2), the secondary beam of neutrons is then incident on a 2 cm thick liquid hydrogen target. The space between the CHARGEX exit window and FEV2 is filled with shielding material that defines a 3.81 cm (H) $\times$ 5.08 cm (V) "doorway" aperture. A "picture frame" veto around that doorway acts as an active collimator. Deuterons and elastically scattered protons produced in the $LH_2$ target pass through a segmented trigger scintillator (FET), then through three sets of front end wire chambers (FECs), and finally are momentum analyzed in SASP. Data from the FECs determine the scattering angle and position at the target of the scattered particles. Scintillators in the focal plane of SASP provide $dE$ information and the start signal to the acquisition electronics. Vertical drift chambers, also at the focal plane, determine the momentum of the scattered particles.

The front end chambers are MWPCs consisting of three sets of paired chambers with each set having two orthogonal planes and a wire spacing of 1 mm. The upstream and downstream sets of chambers, FECM and FEC0, are separated by 330 mm. This wire-plane separation and wire spacing give an angular resolution of better than 0.2° (fwhm) and a position resolution of less than 0.30 cm for the scattered particle. The third set of MWPCs, positioned between the other two and oriented at 40°, is required in order to resolve ambiguities in multi-track events. This chamber, referred to as EFF, also provides redundant information so that chamber efficiencies can be monitored.

We use the $pp \to d\pi^+$ reaction to determine instrumental asymmetries due to the spectrometer acceptance and spectrometer focal plane detection efficiency. While many of these effects, such as energy loss and multiple scattering, are dependent on energy and/or momentum, it is the difference in these dependencies for the two sets of deuterons that is relevant. The complete GEANT based simulation (see the next section) is needed to address these issues.

A schematic of the experimental layout for this calibration reaction is shown in Fig. 29 and is quite similar to the layout for the CSB measurement. A 293.5 MeV proton beam of $5 \times (10)^6$ protons/sec is incident on the $LH_2$ target. In order to measure the instrumental asymmetry for the $np \to d\pi^0$ reaction, the detection system is identical to that used for the $np \to d\pi^0$ measurement. The one exception to this is a hevimetal beam blocker placed upstream of the VDCs, at a position along the focal plane to block the primary and

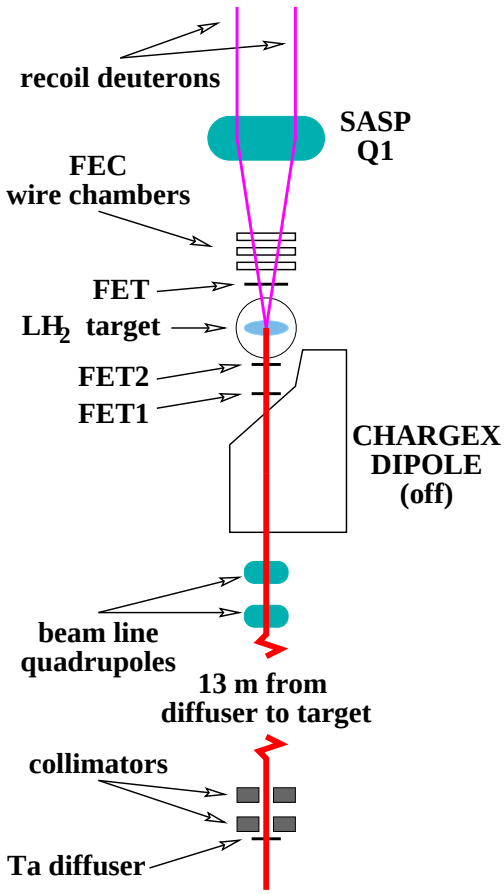


Fig. 29. Schematic drawing of the experimental layout for $pp \to d\pi^+$ measurement showing the collimation and beam line quadrupoles used to produce the low intensity proton beam.

forward scattered protons. This is to protect the VDCs and eliminate these protons from our event stream. The FEV1 and FEV2 scintillators in the front end are now used as trigger scintillators.

**Simulation**

The GEANT simulation of both the $np \to d\pi^0$ and $pp \to d\pi^+$ reactions is well advanced for the front end and focal plane areas of SASP. The key features for the event generator and front end description are:

- generates a nucleon upstream of the target in the lab frame
- tracks the nucleon to a random position in the target ($x$,$y$, and $z$)
- at that position the nucleon disappears with its kinetic energy and 3-vector momentum being saved
- transforms to the cm frame and generates a deuteron using the cm cross section and the initial momentum/energy from the nucleon
- transforms to the lab frame
- tracks the deuteron through the front end (exit of FEC0).

The energy distribution of the incident nucleon is described by a double gaussian if the nucleon is a neutron, or a single gaussian if the nucleon is a proton. By simultaneously fitting these functions to the deuteron kinematic locus and the band resulting from elastically scattered nucleons we expect to determine the average incident beam energy to better than $\pm 5$ keV.

The centre-of-mass cross section for $np \to d\pi^0$ is given by

$$d\sigma/d\Omega = A_0 + A_1 P_1(\theta^*) + A_2 P_2(\theta^*),$$

where $\theta^*$ is the deuteron c.m. angle and $P_i$ are Legendre polynomials. This is the function used to generate the deuterons in the simulation. In this expression, the second term describes any charge symmetry breaking with the coefficient $A_1$ giving the asymmetry. The ratio of $A_0/A_2 = 0.2164$ was obtained in Expt. 466; ultimately we will determine the value of $A_0/A_2$ that best reproduces the data.

Extensive tests have been done to test the integrity of the random number generator and the reproducibility of the code on a new ALPHA machine. Energy loss and multiple scattering in the materials in the front end have also been included. The simulation also corrects for non-zero incident angles. The description of the focal plane detectors is also complete. The next step will be to combine the front end and focal plane routines, and add the acceptance cuts.

**Hardware development**

**Front end chamber gas**

The FECs were designed to run with "magic gas", an argon-isobutane mix with an additional 2% freon. This small percentage of freon allows the chambers to run at a relatively lower voltage and still have a high gain. Due to concerns regarding freon and the UV shielding ozone layer in the upper atmosphere, legislation now exists that strongly regulates the use of freon. Consequently, TRIUMF cannot acquire more of this gas. As the amount of freon existing on site is estimated to last no longer than the end of 1997, we investigated the possibility of running with only argon and isobutane.

Bench tests during spring 1997 suggested that a 30:70 mixture of argon:isobutane would allow stable operation of the FECs. However, when exposed to beam in the proton hall the FECs had difficulty holding voltage and experienced a number of voltage trips that resulted in at least three broken wires. To avoid further

damage to the FECs we 1) returned to magic gas at a reduced flow rate and 2) moved the FEC HV supplies into the experimental area to reduce the length of cable between the power supply and the FECs. Both of these changes have the effect of reducing the amount of energy stored in the FEC system and consequently reduce the amount of energy released in the FECs on each trip. The FECs were stable with this mixture; we had very few chamber trips even with 450 nA of 281 MeV protons in our primary beam. With the supply of freon essentially exhausted, we will investigate alternative gas mixtures in the early part of 1998.

**Upgrade of TDC PROMs**

The FASTBUS TDC readout system for the FECs has been highly unreliable since we received it from LeCroy. In 1996 we identified a hardware problem LeCroy had in one of their Xilinx (programable) chips and replaced those chips. With that problem resolved we became aware of yet another failure due to firmware. At times (particularly after a power glitch) the TDC's need to be reset. We found that the PROMs that were initially installed in the TDC's (rev F) would only perform the initialization on power-up of the FASTBUS crate. Thus, resetting the TDC's required an access into the area and resulted in lost time.

LeCroy issued a new version of these PROMs (rev I) which we bench tested in the spring. These tests confirmed that the new PROMs did allow reinitialization of the TDC's without power cycling the FASTBUS crate. However, the TDC's could not be cleared at high event rates. As fast clearing is essential to this experiment we returned to the original rev F PROMs. To eliminate entering the hall to power-up the crates when reinitializing them, we installed hardware to remotely power cycle the crates.

**Background elimination**

Although the background in our data was reduced by enlarging the cross sectional area of FEV1 and FEV2, there still remained a background from deuterons produced via $C(n,d)$ reactions in FET and in the windows of the $LH_2$ target. Comparisons with various thicknesses of $CH_2$ added at the target position indicate that of the 0.125 in. thickness of FET, only 0.040 in. are active and produce a signal. The remaining ~0.080 in. did not aid in our trigger but did act as a source of background.

Based on these observations we redesigned the front end shielding, FEV2 and FET. We replaced the Cu of the front end shielding with Hevimet and redesigned it for ease of installation. The area of FEV2 was increased to cover the doorway more adequately and veto deuterons being produced in the doorway edges. A new FET was made having the same cross sectional area but half the thickness of the original FET. These had a beneficial effect on the background in that the (signal:background) ratio in the $np \to d\pi^0$ data taken after these changes were made in May was (5.9:1). Improving the timing of the electronics for our summer running reduced the background further, giving a (s:b) of (7.5:1). This is to be compared to the (s:b) of (4:1) seen in December, 1996. Figure 30 shows the kinematic locus for deuterons from the $np \to d\pi^0$ reaction obtained with these improvements.

**Acceptance**

The acceptance of SASP is a function of $(\theta_i,\ x_i,\ \phi_i,\ y_i, \delta)$, the angles and positions of the production vertex on the target and

$$\delta = \frac{p - p_0}{p_0},$$

where $p$ is the momentum of the detected particle and $p_0$ is the central momentum of the spectrometer. This acceptance is further complicated by the non-trivial shape of the spectrometer apertures and appeared to be affected by a correlation in $y_i$ and $\delta$. A new tune of the SASP entrance quadrupoles was expected to reduce the effect of this correlation and $np$ elastic data at three different beam energies were taken to investigate this tune. The different beam energies were required so that the magnetic fields could be kept constant and the beam still sample various portions of the focal plane. The beam energies yielded protons with $\delta$ equal to $-4\%$, $0\%$, and $+4\%$, relative to the central momentum of the deuterons from $np \to d\pi^0$. We obtained between 2 and 3 million events at each energy which allowed a thorough investigation of the acceptance.

The goal of the $np$ elastic data analysis was to map out the relative acceptance (for low momentum vs. high) as a function of $x_i$ and $y_i$ over a large range

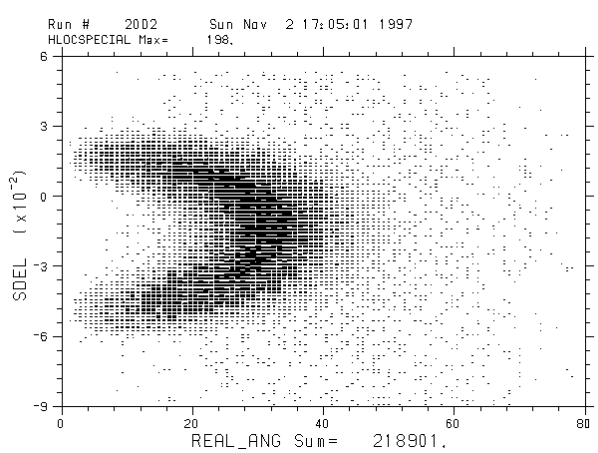


Fig. 30. Kinematic locus of deuterons from $np \to d\pi^0$, summer running period.

of both $x_i$ and $y_i$. The primary purposes of this calibration were two-fold: First, to determine cuts on the SASP target variables which sharply define the spectrometer's phase space, thus providing a common ground for comparison of analysis and simulation. Second, with these cuts in hand, to map out the SASP relative transmission probability (low momentum compared to high momentum) for particles populating various portions of the target variable phase space. To determine appropriate target angle cuts, we examined 2D histograms of the $(\phi_i,\ \theta_i)$ distributions over a grid of "boxes" in the SASP $(x_i,\ y_i)$ target position. Vertices of lozenge-shaped polygon cuts in the $(\phi_i,\ \theta_i)$ plane are found to depend upon the $y_i$ (horizontal position) value and shift in $\phi_i$ as $y_i$ shifts. Based on previous studies, the shape of the lozenges and positions of the vertices were taken to be independent of $x_i$. Only the events passing the cut are considered to fall within the software description of the SASP acceptance. Analysis indicated that the high statistics of the $np$ elastic data permit a correction for the acceptance effect at roughly the $6 \times 10^{-4}$ level for both $x_i$ and $y_i$ ranging between $\pm 2$ cm.

The transformation of solid angle from the lab to the centre-of-mass frame depends upon the beam energy and whether the deuteron momentum is the higher or the lower of the two possible values. If we assume no forward-backward asymmetry in the centre of mass, and use the deuteron distribution determined by Expt. 466, this difference in solid angle transformation gives a ratio of 1.142 for high momentum deuterons to low momentum deuterons, when the lab scattering angle is limited to less than 10 mrad. The value of this ratio, which we will refer to as $R$, is an indication of the momentum dependence in the acceptance and our ability to correct for it. The value of $R$ for the August $np \rightarrow d\pi^0$ data is $1.23 \pm 0.025$ with no acceptance correction. When the corrections extracted from the $np$ elastic data are applied this ratio drops to $1.13 \pm 0.023$. The bottom plot in Fig. 31 shows these data.

However, during detailed studies of this correction in December, it became apparent that the correction was inappropriate in a local sense and, in fact, also depended on $x_i$. Thus, the correction extracted from the $np$ elastic data was only correct as a global average and the agreement between the corrected value of $R$ and the expected value was fortuitous. After extensive $x_i$-dependence investigations, it appears that this dependence is due to problems in properly reconstructing tracks in the VDCs. This is still under investigation.

**Sensitivity to systematic effects**

In parallel with the development of a full GEANT based simulation, we also developed a simple Monte Carlo (SMC) of the $np \rightarrow d\pi^0$ reaction to investigate

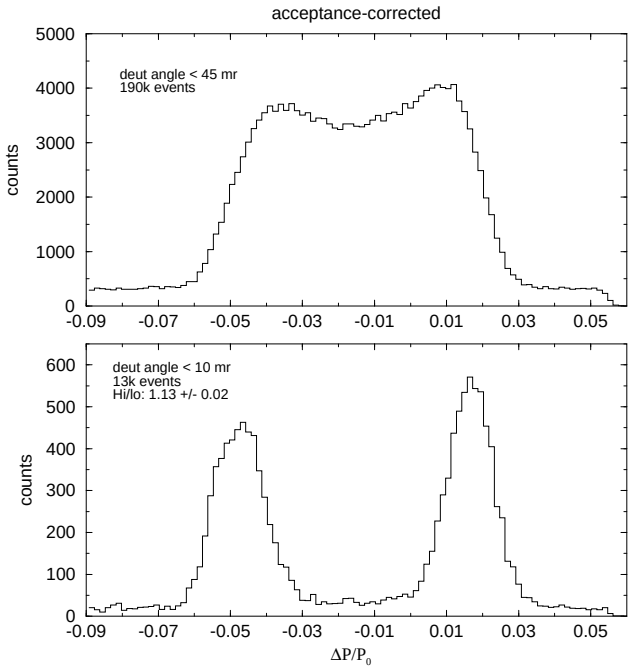


Fig. 31. Acceptance corrected momentum distribution for deuterons from $np \rightarrow d\pi^0$, August. The plot at the top is for $\theta_{\rm scatt}$ <45 mrad (the kinematic limit) and the bottom plot is for $\theta_{\rm scatt}$ <10 mrad.

the sensitivities to some systematic effects. This SMC does not have the level of detail of the GEANT simulation, but includes the following effects:

- the neutron beam energy is chosen according to a gaussian distribution with $E_{\rm cent} = 279.5$ MeV, and $\sigma(E) = 0.5$ MeV
- multiple-scattering effects are included by adding a gaussian distribution to both $\theta_i$ and $\phi_i$
- positions in the $(x_i,\ y_i)$ space are random with a uniform distribution in the standard ($\pm 2$ cm by $\pm 2$ cm) spread.
- distribution of deuteron scattering angles in the centre of mass are chosen according to the Legendre polynomial function in $\cos(\theta^*)$, with an optional non-zero $A_1/A_0$
- the 2D locus produced by the SMC currently has the same dimensions ($100 \times 100$) and limits in $\delta$ and $\theta_{\rm lab}$ as the standard analysis code.

The random number generator used in the SMC has also been exhaustively tested for robustness.

The SMC has been used to investigate the sensitivity of our $\chi^2$ to changes in various parameters. The parameters checked thus far include beam energy and $p_0$. The $\chi^2$ for the fit is defined as follows:

1. Run the SMC once with the "nominal" values for all parameters: $E = 279.5 \pm 0.5$ MeV, $A_1/A_0 = 0.0$, etc. Refer to the spectrum thus generated as the "standard" locus.

2. Rerun the SMC for a different set of parameters. On a bin-by-bin basis, calculate the $\chi^2$ via the definition

$$\chi^2 = \sum \frac{(\text{counts} - \text{counts}_{\text{standard}})^2}{\text{counts}_{\text{standard}}}$$

where the sum is over all bins which have non-zero counts in the standard spectrum.

**Sensitivity to beam energy**

The SMC was carried out 10 times with beam energies varying in 50 keV steps, and the $\chi^2$/bin vs. beam energy extracted. In this pixel-by-pixel scheme, we are very sensitive to the beam energy. To investigate the uncertainty in $A_{fb}$ induced by the beam energy uncertainty, we used the following definition of $A_{fb}$

$$A_{fb} = 2 \times \frac{(R-1)}{(R+1)}$$

where $R$ is the ratio of (high momentum deuterons/low momentum deuterons) with a maximum lab $\theta_{\text{scatt}}$ of 10 mr. Deviations from the value at the standard energy would then represent the error in our understanding of the beam-energy-induced asymmetry for a 10 mr angle-cut. The ratio $R$ may be calculated analytically from the reaction kinematics for arbitrary beam energies above threshold; the resulting deviation from the asymmetry at the standard energy is plotted in Fig. 32 over a $\pm 100$ keV range. For a 25 keV deviation from the "true" energy, we find from the plot that the "false"

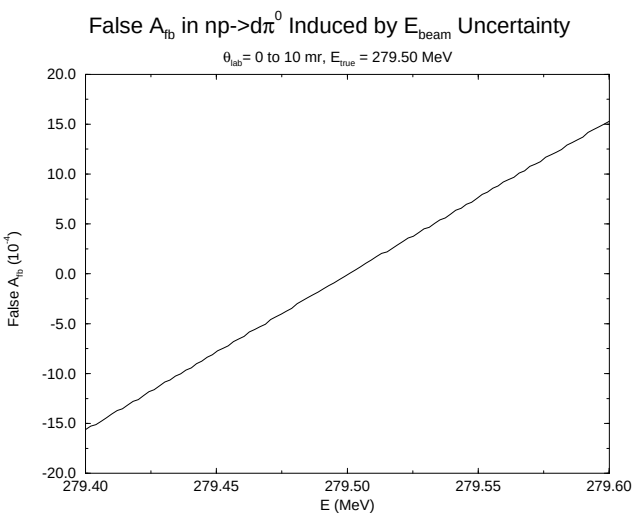


Fig. 32. Systematic effect on $A_{fb}$ due to beam energy uncertainty.

$A_{fb}$ induced by this beam energy difference is about $4 \times 10^{-4}$. We expect the statistical uncertainty in beam energy to be small – 5 keV – so the effect will remain a small contribution to the overall error budget.

**Sensitivity to background**

Subtraction of background under our kinematic locus can introduce both systematic and statistical errors. The statistical uncertainties involve estimates based on target-empty runs or from regions outside the locus. A simple estimate based on background visible in a 1-D projection (onto the momentum axis) of the kinematic locus (top plot of Fig. 31) is that the signal to background ratio is approximately (7.5:1).

Then, assuming the optimal amount of time on target empty for a given amount of total time, we determined the uncertainty in $A_{fb}$ due to the fact that we must subtract a flat background from the simple locus model. The contribution of statistical uncertainty of background subtraction to the uncertainty in $A_{fb}$, given a 7.5:1 signal/noise, is roughly $3 \times 10^{-4}$ according to a simple locus (1-D in $\delta$) model.

From inspection of Fig. 30, we may estimate that in a 2-D fit the background under the locus would be less than in the projected spectrum, at a level of about 10:1 signal to background.

**Sensitivity to acceptance**

Correction of $np \to d\pi^0$ data (based upon $np$ elastic data with the statistics achieved in the August running period) can be made at the level of $6 \times 10^{-4}$ over an $(x_i,\ y_i)$ box of (–2,+2) × (–2,+2) cm. The uncertainty quoted is derived from the statistical uncertainty in the acceptance ratios per bin of the ($\text{tgt}_{\text{pos}}$, $\text{tgt}_{\text{angle}}$, $\delta$) phase space, with a linear interpolation as a function of $\delta$ for corrections between the extremes of $\delta$ (i.e. the $\pm 4\%$ points relative to the 0% point, the two sets of ratios we have in hand from the $np$ elastic running) and 0%.

**Sensitivity to VDC efficiency**

We have developed a method of measuring the SASP VDC efficiency as a function of momentum, which is required for this measurement of $A_{fb}$. The method relies on a prediction of position in a given VDC plane ($X1$, for example) based upon the position and internal angle information from the "complementary" plane (e.g. $X2$). In the full analysis the single-plane inefficiency is expected to be less than 1%. However, the statistical accuracy of the efficiency-per-bin method will be barely sufficient to determine the efficiency vs. $\delta$ of the SASP focal plane on a run-by-run basis. A sum over several runs, however, will be adequate to determine the efficiency profile – that is, to detect changes in single-wire VDC efficiency on the

timescale of a few runs. The systematic uncertainty in $A_{fb}$ due to VDC efficiency is only 25% as large as the statistical uncertainty in $A_{fb}$.

**Data acquisition**

During 1997 we used beam to study the properties of the low intensity proton beam and test the reproducibility of this beam. We also confirmed the ease and reliability of interleaving the two phases of the experiment. The *np* elastic data, which are needed to determine the acceptance of SASP, were also taken during this year. By the end of 1997 we had obtained approximately 2,400,000 $pp \to d\pi^+$ events and 544,000 $np \to d\pi^0$ events. This was in spite of being required to remove and reinstall most of the equipment associated with the experiment due to another experiment running on beam line 4B.

## Experiment 714
## Atomic PNC in francium: preparations

*(P. Dubé, SFU; J.A. Behr, K.P. Jackson, TRIUMF)*

We attempted to trap $^{226}$Fr produced from TISOL in a Zeeman optical trap. Due to our limited collection efficiency of $1 \times 10^{-3}$ and difficulties with relatively poor production from the TISOL target, this attempt failed. However, a significant milestone was reached when we learned to precisely lock the Ti::sapph laser frequency to the Fr frequency at 718 nm, by using saturation spectroscopy of the iodine $I_2$ molecule. This is a relatively common technique at shorter wavelengths in $I_2$, but the absorption lines in the near infrared are much weaker, and to our knowledge this has not been done before.

**Stabilization of a Ti:sapphire laser using the hyperfine structure of molecular iodine.**

Cooling and trapping depend directly on the detuning from the atomic transition line centre, thus it is important to be able to stabilize the laser frequency to a fraction of the ≈10 MHz atomic linewidth. When compared to the optical frequency of 400 THz, this amounts to a relative stability of about 1 part in $10^8$ during the course of an experiment.

A second aspect of the problem is to tune the absolute frequency of the laser to that of the transition. The position of the trapping transition in $^{226}$Fr is known to ±60 MHz [Bauche *et al.*, J. Phys. B: At. Mol. Phys. **19**, L593 (1986); Coc *et al.*, Phys. Lett. **163B**, 66 (1985)], so it is to our advantage to know the laser frequency to that accuracy, and preferably better to avoid contributing to the uncertainty in the position of the line, and therefore the search time. In reality, it has been found in some cases that the numbers given in the literature differed by nearly $3\sigma$ [Lu *et al.*, Phys. Rev. Lett. **79**, 994 (1997)], thus increasing our search range threefold to about 360 MHz.

We have chosen $I_2$ both as an absolute frequency reference and to stabilize the laser. This is a logical choice for several reasons; $I_2$ was used in the previous measurements of the francium isotopes' optical transitions. It also has a line in coincidence with the $^{226}$Fr trapping frequency: the centre of gravity of the $I_2$ line number 379 [Gerstenkorn *et al.*, Atlas du spectre d'absorption de la molécule d'iode, 11000 cm$^{-1}$ – 14000 cm$^{-1}$, Laboratoire Aimé Cotton CNRS II 91405 Orsay, France (1982)] is located at −42(80) MHz from the $^{226}$Fr cycling transition (F=3/2→F′=5/2).

The $I_2$ line #379, the P86(1-9) transition in the B-X electronic system of $I_2$, is about 1.3 GHz wide due to Doppler broadening and hyperfine structure. We have performed saturation spectroscopy on this $I_2$ line to obtain a Doppler-free spectrum composed of 15 hyperfine transitions, resolved into 12 components. These components were our markers for controlling the laser frequency, instead of the very broad Doppler broadened profile. Figure 33 shows the hyperfine spectrum of line 379 that we have obtained by saturation spectroscopy. Each hyperfine transition had a linewidth of ≈5 MHz, mostly from pressure broadening. (The natural linewidth would be ≈1 MHz.)

All the requirements stated above are thus met if one can lock the laser to individual hyperfine components: their widths were 5 MHz, and so it was trivial to get a stability of better than 1 MHz with even a poor lock, and the position of the centre-of-gravity of those lines was well known, as discussed above. To lock the laser to any of the hyperfine components, we have dithered the laser frequency using an acousto-optic modulator and recovered the dispersion lineshapes with lock-in detection. The dispersion signals were then fed to a servo loop to keep the laser frequency at line centre. Other acousto-optic modulators

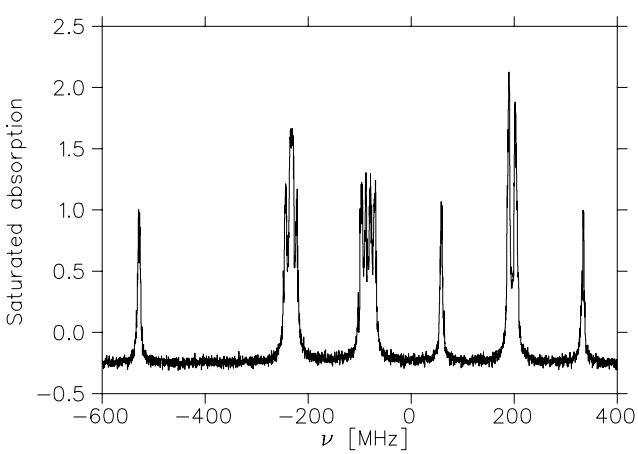


Fig. 33. Saturation spectroscopy at 718 nm in $I_2$.

tuned the laser frequency from the fixed points given by the hyperfine components, which allowed precise scanning across the range where the francium trapping resonance was expected to be located.

The transitions at 718 nm are from excited states, so the quartz cell must be heated to 400°C. The technique can be applied without expensive modulators to lock the trap laser to $^{221,212}$Fr, which also lie within Doppler-broadened $I_2$ lines (but require an additional laser for repumping light). We have also shown that the technique can be used to lock the laser to $I_2$ lines near the 767 and 770 nm transitions in natural potassium, which would be useful for trapping $^{36}$K and $^{38}$K ground state in possible future experiments. It remains a useful precision spectroscopic reference for the even weaker lines at 817 nm, the D1 wavelength of Fr, a useful repumper diode laser wavelength.

**Experiment 715**
**Weak interaction symmetries in $\beta^+$ decay of optically trapped $^{37,38m}$K**
*(J.A. Behr, K.P. Jackson, TRIUMF; O. Häusser, SFU/TRIUMF)*

We have demonstrated that we can detect recoil-$\beta^+$ coincidences from the decay of 0.925 sec isomeric $^{38m}$K and 1.226 sec $^{37}$K at rates sufficient to make a preliminary measurement of $\beta$-$\nu$ correlations possible. Further progress has been hindered by our poor collection efficiency, which we must now address further.

**Search for scalar currents with $\beta$-$\nu$ correlation**

For $\beta$-decay studies, the Zeeman-optical trap (ZOT) provides a sample of atoms in a localized volume with virtually zero source thickness, so unperturbed nuclear recoils can be detected in coincidence with the $\beta$, allowing the determination of the $\nu$ momentum. In the $0^+ \rightarrow 0^+$ Fermi decay of $^{38m}$K the leptons carry away no net angular momentum. Unlike the standard model (V-A) interaction, mediated by the $W$ vector boson exchange, a scalar interaction would demand like helicities for both leptons and antileptons. Thus for vector bosons back-to-back emission of the leptons is forbidden, while back-to-back emission is maximal for scalar boson exchange. We measure back-to-back coincidences between $\beta^+$ and $^{38}$Ar neutral atom recoils; the recoils will have lower energy – hence longer time of flight – if the leptons are emitted back-to-back. In addition, we collect charged Ar recoils with high efficiency with a uniform electric field, and reconstruct their angular distribution.

Limits on the scalar interaction are poor, both from beta decay [Adelberger, Phys. Rev. Lett. **70**, 2856 (1993); Erratum, Phys. Rev. Lett. **71**, 469 (1993)] and from particle physics. A 1% measurement of the $\beta$-$\nu$ correlation coefficient $a$ would be competitive.

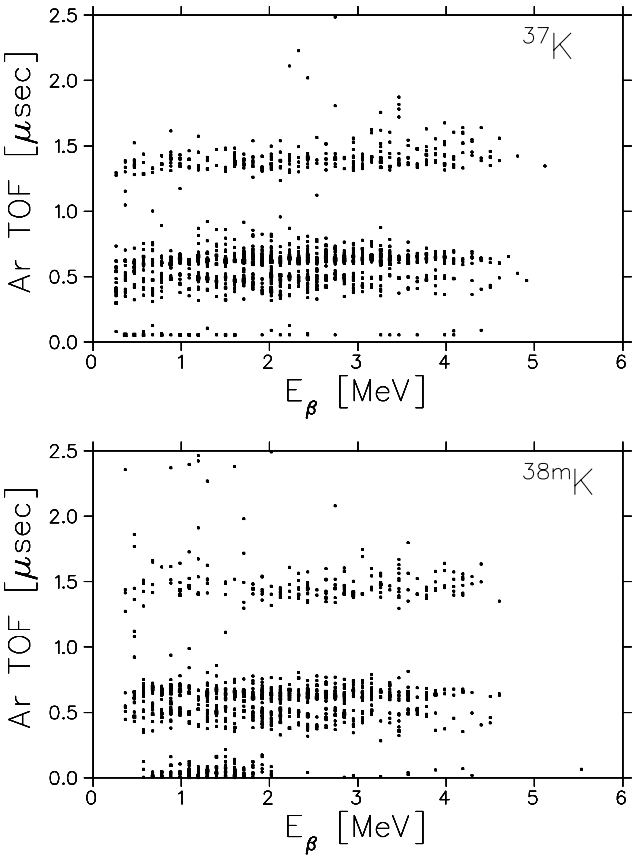


Fig. 34. Scatter plot for Ar recoil TOF vs. kinetic $E_{\beta+}$. 200 atoms trapped, 1 day each. $|\vec{E}| = 800$ V/cm separates $Ar^0$, $Ar^{+1}$, $Ar^{+2}$ in TOF.

Figure 34 shows scatter plots of Ar recoil TOF vs. $\beta^+$ energy, showing $Ar^0$, as well as $Ar^{+1,+2,+3}$ accelerated by the uniform electric field. The spectra are for roughly equal numbers of decays, so for events with $E_\beta \geq 2.5$ MeV, the suppression of the lower energy recoil branch in $^{38m}$K compared to $^{37}$K is qualitatively apparent. (The slow $Ar^0$ events with $E_\beta \leq 2.5$ MeV are kinematically forbidden, and are due to $\gamma$-ray background – see below.) The large (≈20%) microchannel plate (MCP) efficiency for neutral Ar atoms, given their very low kinetic energies of 0–450 eV, is probably due to metastable Ar atomic states. Two of the first four excited states at 11.5 eV (sharing $3p^5 4s$ configuration) are metastable (with lifetimes 38 and 0.1 sec): many excited states of Ar decay feed these four states, and statistical population of these states would yield 50% metastables. As such, the efficiency would in principle vary little with kinetic energy, but this will be very difficult to quantify. From literature data, the accelerated $Ar^{+1,+2}$ recoils will be detected with equal probability (≈ 60% of the solid angle, determined by the areal density coverage of MCP channels) to within a few percent.

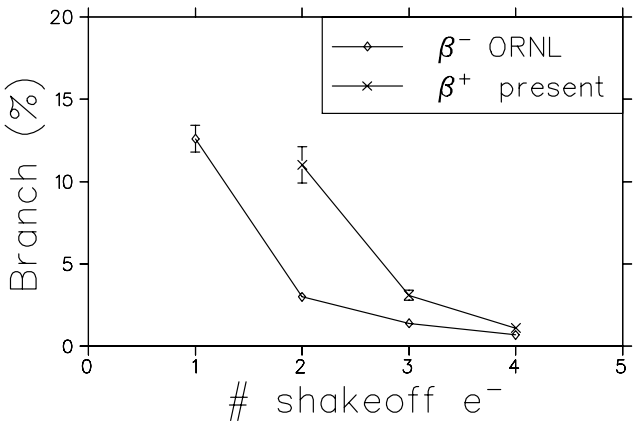


Fig. 35. Measured charge state distribution of Ar produced in $^{37}$K decay, and charge state distribution of $^{41}$K produced in $^{41}$K $\beta^-$ decay [Snell *et al., op. cit.*].

Ours are the first measurements of charge state distributions in $\beta^+$ decay. Figure 35 shows our results, along with ORNL data from $\beta^-$ decay of $^{41}$Ar [Snell *et al.*, in $\alpha$-,$\beta$-, and $\gamma$-ray spectroscopy, K. Siegbahn, ed. (1964)], as a function of the number of shakeoff electrons. Phenomenologically, it appears that a better figure of merit would be to compare final atomic configurations (e.g. $K^{+1}$ to $Ar^{+2}$).

**Technical progress**

Small changes in the neutralizer geometry have not increased the capture efficiency of $\approx 10^{-3}$. Adding large quantities of Rb vapour (as is necessary to cure defects in the Dryfilm non-stick coatings at JILA [Lu *et al.*, Phys. Rev. Lett. **79**, 994 (1997)], enabling them to achieve 50% trapping efficiency) has only hurt the capture, by damaging the ionizing parts of the present neutralizer. Using a hot wire technique, we find that $\approx$15% of the ions are converted into neutral atoms in the cube region, a small result. Raising the neutralizer temperature higher, to allow quicker diffusion of the short-lived isotopes, also destroys the Dryfilm on 2–4 week timescales (this occurred during beam time in November-December).

Inspired by recent LANL success in trapping $^{82}$Rb from an ion beam [Vieira, private communication], we are radically changing the design, moving the neutralizer to the far side of the cube, and transporting the ion beam through the trap region to the neutralizer. Atoms desorbing from the surface will directly enter the cube. This has several advantages. The metal surface now only needs to neutralize; since alkali deposits lower the work function, the neutralizer should now be compatible with the Rb needed to cure the Dryfilm. A material to optimize diffusion and release times can be chosen. A steeper angle of incidence will mean a smaller average implantation depth into refractory metals. We will also test alkali metal neutralizers at close to room temperature: literature data indicate diffusion times in Rb, Na or Li neutralizers would be $\leq$0.1 s, and adsorption enthalpies from semiempirical calculations also suggest short desorption times. The goal is to achieve total efficiencies of 5%, limited in this geometry by the 6 mm holes needed for the TISOL beam. Smaller holes with the smaller emittance beam from ISAC could increase this further.

We have moved the second trap farther away to allow for more $\gamma$-ray shielding, to minimize random firing of the MCP from $\gamma$-rays from the ground state of $^{38}$K, which is left behind in the collection trap region. (The $\gamma$-rays can be seen as kinematically forbidden events with $E_\beta \leq E_\gamma = 2.17$ MeV in Fig. 34.) We have maintained $\geq$75% transfer between our two traps by adding a second 2-d magneto-optic funnel.

We have made several detector upgrades. We have changed our MCP from a 2-plate chevron to a 3-plate Z-stack, to improve uniformity of position, angular and energy response by saturating pulse heights. To minimize backscatter tails and improve the full energy efficiency, we have switched from two 5 mm SiLi's to a BC408 plastic scintillator with 7.7% energy resolution at 4.2 MeV, and achieved relative timing of $\leq$1 ns. The scintillator pulse height is stabilized by an LED pulser stabilization circuit courtesy Y. Holler at DESY; a blue LED (450 nm) is used. Upgrades of the double-sided Si strip detector preamps have been completed in conjunction with H. Coombes and the TRIUMF Electronics Shop.

**Optical pumping for $^{37}$K spin correlations**

With the demonstration of >75% transfer efficiency to the second ZOT, the atomic physics development for the $^{38m}$K experiment is basically complete. A laser development lab has been started to work on optical pumping of stable $^{41}$K, to prepare for experiments with polarized $^{37}$K. A possible measurement cycle (of 5 ms duration) would be to trap $^{41}$K atoms in a ZOT, turn off the ZOT, optically pump the atoms as the cloud falls and expands, probe the result with stimulated Raman scattering (and/or, for $^{37}$K, count decays), and restore the ZOT. Detailed calculations of optical pumping at arbitrary $B$ field (made non-trivial by the small hyperfine splitting) have been performed. The trap laser will be a Spectra Diode Labs MOPA seeded with a New Focus low power single mode narrow frequency diode, a combination that is $\approx$5 times cheaper than our standard $Ar^+$-pumped Ti::sapph; the combination will require development.

A detailed simulation has been performed for a geometry including optical pumping beams from alternate directions at 90 degrees, a MCP for recoil collection, and a $\beta^+$ detector, with a measurement strat-

egy for simultaneously extracting the standard coefficients to fully characterize the decay (the $\beta^+$ asymmetry $A$, $\nu$ asymmetry $B$, $\beta^+$-$\nu$ correlation $a$, and tensor correlation $c$). From these, in principle the Gamow-Teller/Fermi mixing ratio can be extracted simultaneously with limits on new physics such as right-handed currents.

**Experiment 719**
**$^4$He($\pi^+, \pi^- pp$) invariant mass measurement with CHAOS**
*(R. Meier, Tübingen; M.E. Sevior, Melbourne; G.R. Smith, TRIUMF)*

This experiment received beam time during the high intensity beam periods of TRIUMF operation in January, July and December 1996. The CHAOS spectrometer with a $^4$He gas target was used in the TRIUMF M11 area. Measurements were done at pion kinetic energies of 115 and 105 MeV.

The experiment is searching for the hypothetical $d'$ dibaryon, which is a possible explanation for the enhancement in the total cross section of pion double charge exchange (DCX) to discrete final states in nuclei around $T_\pi = 50$ MeV. From the analysis of DCX, the mass of the $d'$ has been derived to be about 2065 MeV, with a width of about 0.5 MeV. The quantum numbers were suggested to be $J^P = 0^-$ and $T = 0, 2$. With these quantum numbers, the $d'$ can not couple to the two nucleon channel, but will decay into a pion and two nucleons.

Experiment 719 searches for the $d'$ by investigating the double charge exchange reaction $\pi^+$ $^4$He$\rightarrow$ $\pi^- pppp$. If the $d'$ exists, a large part of the DCX cross section in a region above the $d'$ production threshold should be due to the reaction $\pi^+$ $^4$He$\rightarrow$ $d'pp \rightarrow$ $(\pi^- pp)$ $pp$.

CHAOS was set up to simultaneously detect the $\pi^-$ and at least two protons. From the measured momenta of the three detected particles, the invariant mass of the $\pi^- pp$ system can be calculated; the $d'$ should show up as a peak in the invariant mass spectrum. As only two of the four protons in the final state can possibly come from the $d'$, the peak will be accompanied by a combinatorical background from detecting one or two protons not from the $d'$. Additionally, there will be background from non-resonant DCX.

Although the DCX mechanism via the $d'$ is predicted to dominate the DCX cross section just above the $d'$ threshold (at about $T_\pi = 80$ MeV), the measurements were done at 25 and 35 MeV above threshold. Simulations showed that near threshold for acceptance reasons the signature expected from the $d'$ is indistinguishable from the behaviour of conventional DCX.

The data are presently being analyzed at the Univ. of Melbourne and the University of Tübingen. Preliminary results for the invariant mass spectra are shown in Figs. 36 and 37. In Fig. 36, the data at 115 MeV are compared to the shape expected from $d'$ production (dot-dashed curve) and the conventional mechanism (solid line). Here, using only the conventional mechanism yields the best fit to the data for $d'$ masses between 2050 and 2070 MeV/c$^2$. The $d'$ contribution is smaller than about 15% at a 95% confidence level. This contribution is much smaller than expected from predictions [see Clement *et al.*, Phys. Lett. **B337**, 43 (1994) and Graeter *et al.*, Phys. Lett. **B** (in press)].

In Fig. 37, the data at 105 MeV are compared to results from GEANT simulations for a $d'$ production mechanism (dot-dashed line) and a conventional 2-step single charge exchange mechanism (dashed line). It can be seen that the expected signature for the $d'$ at this energy closer to threshold is less clear than at 115 MeV.

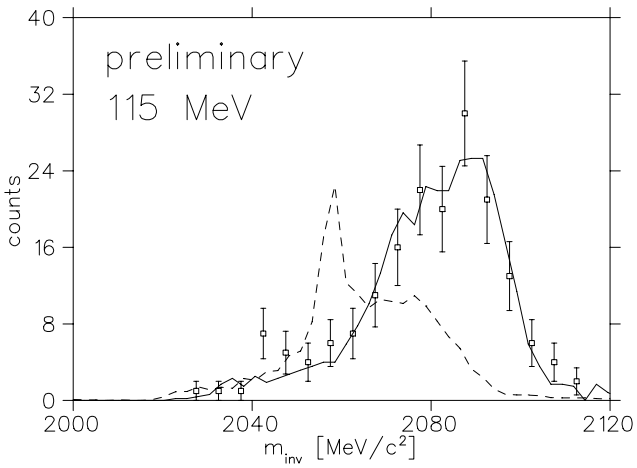


Fig. 36. Preliminary results at 115 MeV. For details see text.

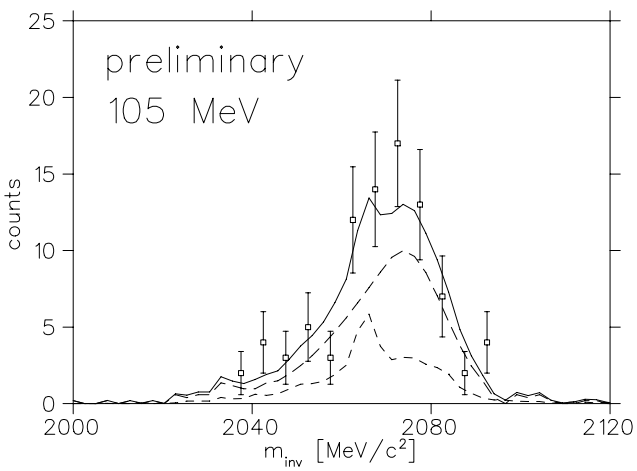


Fig. 37. Preliminary results at 105 MeV. For details see text.

The best fit to the data (solid line) gives a $d'$ contribution of about 25%±25% to the sum (for a $d'$ mass of 2065 MeV/c$^2$).

**Experiment 722**
**Pion initial state interactions in the $^{12}$C($\pi^+, ppp$) reaction**
*(R. Tacik, TRIUMF/Regina)*

Experiment 722 was run in the M11 channel at TRIUMF. Measurements were taken at incident pion energies of 280, 240, and 200 MeV. A thin rod of plastic scintillator was used as an active carbon target. The CHAOS spectrometer was used to measure the angles and momenta of outgoing particles. The CHAOS first and second level triggers were set to accept ≥2 charged particles. Thus, data for many reactions channels were acquired simultaneously.

Data analysis for the $^{12}$C($\pi^+, pp$) and $^{12}$C($\pi^+, ppp$) reactions has been completed, and the results were accepted for publication in Phys. Rev. C (March, 1998). Some of the observations made were that:

- About 25 to 35% of the observed ($\pi^+, pp$) events could be clearly identified as being due to direct two-nucleon absorption.
- About 20 to 25% of the observed ($\pi^+, ppp$) events were well described by a model assuming the two step process of $\pi^+p$ quasielastic scattering followed by direct two-nucleon absorption.
- The momentum and missing-momentum distributions of the remaining ($\pi^+, ppp$) events were best described by a model assuming four-nucleon absorption (4NA), although the out-of-plane angular distribution of these events was not well described by this model. There was no evidence for a strong contribution from a direct three-nucleon absorption (3NA) process.

The first two observations are consistent with the results of other nuclear pion absorption experiments. The last is surprising because analyses of recent pion absorption experiments on $^4$He indicate a strong three-nucleon absorption, and only much weaker four-nucleon absorption. However, this observation is supported by an analysis of the $^{12}$C($\pi^+, pd$) and $^{12}$C($\pi^+, ppd$) data sets which were obtained in Expt. 722.

The solid histograms in the first column of Fig. 38 represent the measured distributions of the sum of kinetic energies of the detected protons and deuterons ($T_p$+ $T_d$ = TSUM$_{pd}$) from the ($\pi^+, pd$) reaction. The arrows indicate the maximum energy available to the two detected particles if the residual nucleus were left in its ground state. The long-dashed histograms in

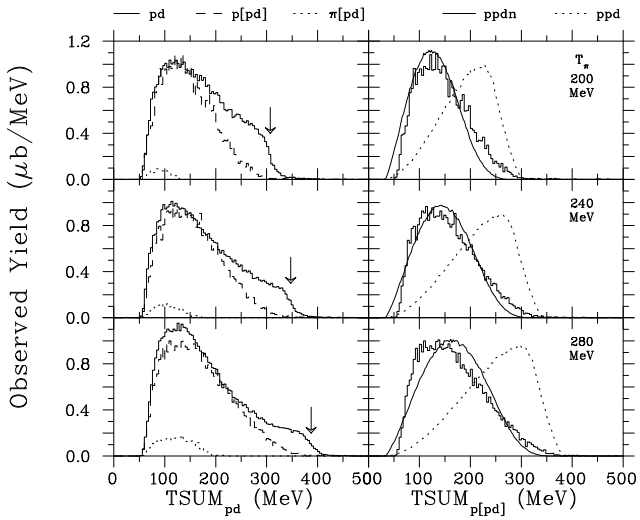


Fig. 38. Summed energy distributions measured in Expt. 722. See text for a detailed explanation.

the first column of Fig. 38 represent summed energy distributions obtained from the measured ($\pi^+, ppd$) events, analyzed by considering the two detected $pd$ final-state pairs separately (referred to as $p[pd]$). The short-dashed histograms in the first column of Fig. 38 represent the summed energy distributions $T_p$+ $T_d$ obtained from measured ($\pi^+, \pi^+pd$) events (referred to as $\pi[pd]$). The sum of the $p[pd]$ and $\pi[pd]$ contributions reproduces the shape of the measured $pd$ distributions quite well at lower values of TSUM$_{pd}$. We find that the events at the higher values of TSUM$_{pd}$ are well described by a model of two-nucleon absorption followed by a final-state pickup reaction.

In the second column of Fig. 38, we once again show the TSUM$_{p[pd]}$ distributions of the $p[pd]$ events, but now compared with the results of simulations using two different models for multi-nucleon absorption. The dotted curves in the second column of Fig. 38 represent the expected summed energy distributions from a 3NA process, which results in a $ppd$ final state. The solid curves in the second column of Fig. 38 represent the results of a 4NA model, resulting in a $ppdn$ final state, in which the $n$ is not detected. It is clear that the large missing energy associated with the measured events is described reasonably well by the 4NA model, and not at all by the 3NA model.

**Experiment 725**
**Pionic double charge exchange on $^4$He**
*(E. Friedman, Jerusalem; G.J. Wagner, Tübingen)*

This experiment of the CHAOS collaboration received beam time during the high intensity periods of TRIUMF operation in February, 1996. The experiment

employed a liquid $^4$He target with the CHAOS spectrometer in the TRIUMF M11 beam line. The data analysis was completed last summer and the main results are due to appear in Physics Letters B early in 1998, to be followed by a full length paper.

In the energy region of the $\Delta$-resonance, the reaction mechanism of pionic double charge exchange (DCX) on nuclei seems to be fairly well understood. In contrast, around 50 MeV the forward angle excitation function for DCX to well-defined final states on light and medium weight nuclei shows a resonance-like structure which is not accounted for by conventional reaction mechanisms.

The hypothetical $\pi NN$ resonance $d'$ was proposed as a possible explanation of this peculiar energy dependence in DCX to discrete final states in nuclei. According to this hypothesis the observed behaviour corresponds to the formation of the $d'$ in the course of the DCX process. The parameters of the $d'$ deduced from DCX to final states in nuclei are $m \approx 2.06$ GeV/c$^2$, $\Gamma_{\pi NN} \approx 0.5$ MeV and $I(J^P) = \text{even}(0^-)$. The pionic DCX reaction on $^4$He is of interest regardless of the $d'$ hypothesis because no cross section data exist for this reaction below 100 MeV, whereas for other light nuclei with $A > 6$ there are ample data displaying the above mentioned structure. In the present work we have measured the inclusive DCX cross section for incoming pion kinetic energies between 70 and 130 MeV. The lower energy is below the $d'$ threshold and at 130 MeV the $d'$ contribution is expected to be small. Around 90 MeV, conventional models predict cross sections that differ by as much as one order of magnitude from predictions based on the $d'$ hypothesis. As a possible additional test of the reaction mechanism we also measured the momentum distributions of the outgoing pions because it is expected that a strong attractive final state interaction (FSI) between protons from the $d'$ decay is effective.

The measurements were performed on the M11 channel at TRIUMF using the CHAOS detector and a liquid $^4$He target developed at the Univ. of Regina. The total cross section of the $^4\text{He}(\pi^+,\pi^-)$ reaction was determined by detecting outgoing negative pions over the full 360° within the scattering plane, and extrapolating the finite acceptance to $4\pi$. The data were normalized to $\pi^+$-$^4$He elastic scattering. The measured quantities in this experiment were the angle- and momentum-dependent yields of outgoing negative pions for the DCX reaction and of positive pions for the elastic scattering. The differential cross sections for elastic scattering of positive pions on $^4$He are available in the literature. By comparing the elastic scattering yields measured with CHAOS to the known cross sections for elastic $\pi^+$ scattering, empirical normalizations were determined and found to be independent of angle. The experimental results of the total cross sections measured in this work are shown in Fig. 39 as solid points. The errors shown are statistical and systematic errors added quadratically.

For the theoretical description of the DCX on $^4$He within a conventional reaction mechanism we first use a model by Gibbs and Rebka, assuming a sequential single charge exchange process (SCX) for the reaction. The results of this calculation (dot-dashed line in Fig. 39) yield only a qualitative agreement with the data at energies above 120 MeV and are an order of magnitude smaller than our data at lower energies. However, before associating such a failure with a non-conventional process, we note that the final state interaction (FSI) between the outgoing nucleons which is expected to lead to an enhancement of the cross section at low energies, is not included in that calculation. Since there is no simple and clean way to include FSI effects in that fully quantum mechanical calculation, we have chosen an alternative way to calculate the DCX reaction.

In this alternative, semi-classical model (dotted curve in Fig. 39), the DCX reaction $^4\text{He}(\pi^+,\pi^-)pppp$ is simulated as a sequential SCX reaction using a Monte Carlo approach, where energy shifted experimental SCX cross sections are used. In addition to the Pauli principle a Watson-Migdal-type FSI has been taken into account both between the two active nucleons and between the two spectator nucleons. This model needs a normalization constant which we find by

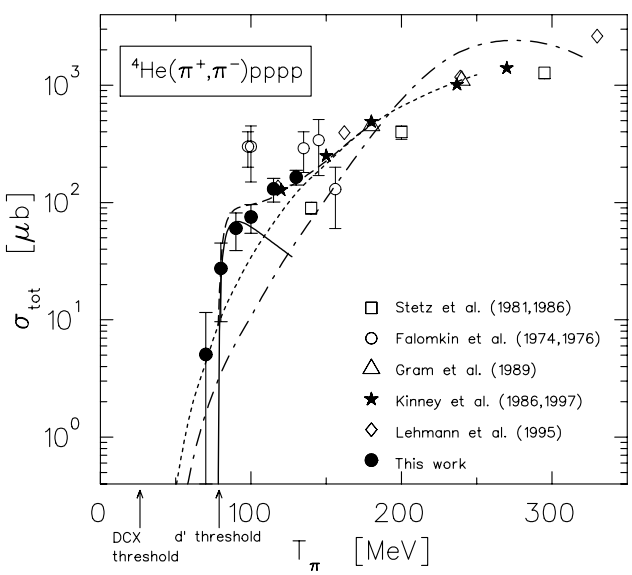


Fig. 39. $^4\text{He}(\pi^+,\pi^-)$ total cross sections. The dot-dashed curve shows results from the Gibbs-Rebka model, the dotted curve represents the MC model, the full curve the $d'$ mechanism and the dashed curve the incoherent sum of the MC model and the $d'$ mechanism.

normalizing the calculations to the data at 180 MeV. Figure 39 shows (dotted curve) excellent agreement between this calculation and all the data above 150 MeV, suggesting that our MC approach provides also a reliable estimate of the conventional DCX cross section at lower energies. Here our MC approach gives a substantially larger cross section compared to the Gibbs-Rebka prediction. This is partly due to the inclusion of the Watson-Migdal FSI effects.

It is seen that for $\pi^+$ energies around 100 MeV the experimental cross sections are significantly larger than the results from the two conventional reaction models discussed above. They are a factor of 3 larger than the MC calculations and an order of magnitude larger than the results of the model of Gibbs and Rebka. In addition, while all conventional calculations predict a smooth energy dependence of the total DCX cross section, the data suggest a sudden rise just above the $d'$ threshold and a peculiar, almost 'knee-like' energy dependence around 90 MeV. The predicted $d'$ contributions to the cross section (full curve in Fig. 39) are clearly capable of improving the description of the data. Indeed, the incoherent sum of the $d'$ cross sections and the cross sections of the MC model describe the data well, as is seen from the dashed line. Of course, this observation can not be construed as definitive proof of the $d'$ hypothesis. On the contrary, the variation represented by the two conventional calculations underscores the inherent model-dependence of any such conclusion. Yet, the fact that the total cross section rises steeply at the $d'$ threshold and both calculations lie well below the experimental results in the region where the $d'$ is expected to dominate is noteworthy, and it supports the $d'$ hypothesis.

**Experiment 741**
**Beta-delayed proton decay of $^{17}$Ne to $\alpha$-emitting states in $^{16}$O**
*(J.D. King, Toronto)*

The goal of this experiment is to obtain an $\alpha$-particle spectrum from the break-up of $^{16}$O following the $\beta$-delayed proton decay of $^{17}$Ne, and to use this spectrum to reduce the uncertainty in the $^{12}$C$(\alpha,\gamma)^{16}$O reaction rate, which is of prime importance in determining the ratio of $^{16}$O to $^{12}$C at the end of helium burning in stars. In Expt. 589 we measured the $\alpha$-particle spectrum from the break-up of $^{16}$O following the $\beta$ decay of $^{16}$N. Through simultaneous $R$- and $K$-matrix fits to this spectrum, to the $^{12}$C$(\alpha,\gamma)^{16}$O data sets, and to $^{12}$C$(\alpha,\alpha)$ scattering data, we were able to reduce considerably the uncertainty in the $E1$ component of the astrophysical $S$-factor for the $^{12}$C$(\alpha,\gamma)^{16}$O reaction, which is determined primarily by the tail of the sub-threshold $1^-$ state at 7.117 MeV. Since the $2^+$ state at 6.917 MeV is not populated in the decay of $^{16}$N, the effect of the tail of this sub-threshold state on the $E2$ component was not determined, and a very large uncertainty in this component, which could be as large as the $E1$, still exists. However, $2^+$ states in $^{16}$O are populated in the $\beta$-delayed proton decay of $^{17}$Ne and the feasibility of using this decay is being explored in this experiment.

During the past year we have continued our investigation of the break-up of the $1^-$ state at 9.59 MeV in $^{16}$O through the detection of proton–$\alpha$–$^{12}$C triple coincidences following the decay of the isobaric analogue state (IAS) at 11.193 MeV in $^{17}$F. A Monte Carlo simulation of the proton decay of the IAS had shown that an optimum arrangement in the laboratory reference frame for detecting triple coincidences would consist of two large area detectors at right angles to each other, with a third large area detector at 110° to one of the first pair. The detector system used in the 1996 run consisted of two 900 mm$^2$ ion-implanted detectors at right angles, and two 450 mm$^2$ detectors placed at 110° to one of the larger detectors (see Fig. 40).

In June and July of 1997 we repeated the triple coincidence measurement with two separate modifications to the detector arrangement. In the first experiment, we replaced detectors F3 and F4 with a 4400 mm$^2$ microchannel plate (MCP) in the chevron configuration and a 3850 mm$^2$ microsphere plate (MSP), respectively. Because of the large solid angle subtended by these detectors, the F1F3 and F2F4 pairs were well-placed (at 160°) to detect protons ($\alpha$'s) and $^{16}$O ($^{13}$N) recoils in coincidence, as well as to record triple coincidences. These data are currently under analysis. In a second experiment detectors F3 and F4 were replaced by two identical double-sided silicon strip detectors of active area 5 cm × 5 cm with 16 strips per side, with adjacent strips connected together to give 64 pixels per

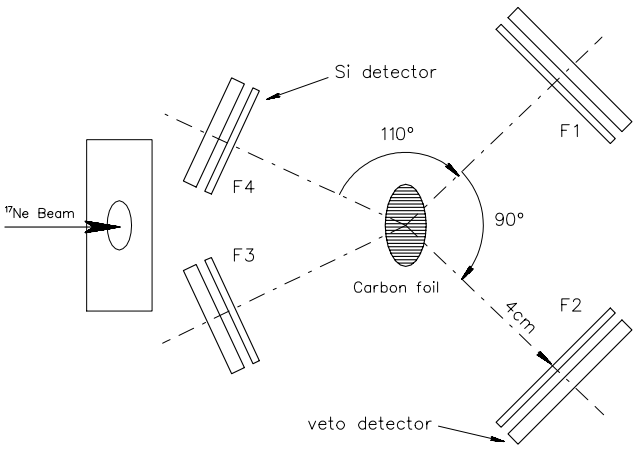


Fig. 40. Detector arrangement for the detection of $p$–$\alpha$–$^{12}$C triple coincidences from the decay of the IAS in $^{17}$F.

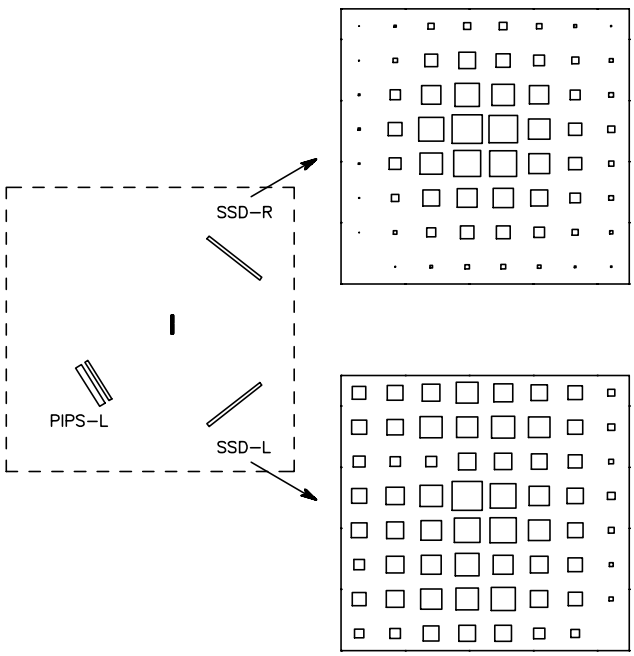


Fig. 41. Hit patterns on the two strip detectors for a triple coincidence with one of the ion-implanted detectors.

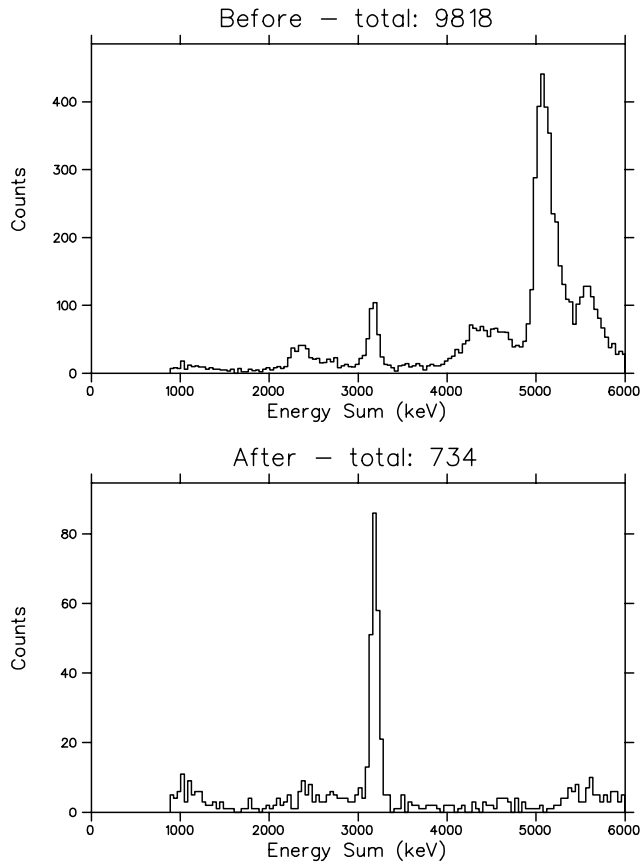


Fig. 42. Triple coincidence energy-sum spectra for a single strip (strip 4) of each double-sided strip detector. The upper panel shows uncorrected data: the lower panel shows a spectrum partially corrected for kinematic effects. See text for details.

detector. In Fig. 41 we show the hit pattern for each of the strip detectors in coincidence with one of the two ion-implanted detectors (PIPS-L≡F3 of Fig. 40) when a gate is set on the IAS peak in the triple sum spectrum. The strip detector SSD-R(F2) has recorded $\alpha$'s and $^{12}$C recoils in coincidence with $^{12}$C recoils and $\alpha$'s, respectively, in PIPS-L, while SSD-L(F1) has recorded the protons in coincidence with the $\alpha$–$^{12}$C pairs. A similar pattern is obtained with PIPS-R(F4) and the two strip detectors, with the hit patterns on SSD-L and SSD-R reversed. This indicates that the geometry is well-chosen for this set of detectors.

In Fig. 42 we show the triple coincidence sum spectrum for two vertical strips of the strip detectors (strip 4 for each) and one of the PIPS detectors. The upper spectrum shows the uncorrected data. The IAS sum peak is clearly visible and the background is quite low, even without the kinematic requirement to remove two-body effects. The lower spectrum has had a preliminary kinematic correction applied to it. The PIPS detector, which recorded the $^{12}$C recoils, had not yet been properly calibrated for these low energy ions. Even with the rather relaxed constraints required to accommodate the resultant uncertainty in the total energy sum, the background due to two-body decays is much reduced.

For the second experimental run a small $\beta$ paddle was inserted into the vacuum chamber but, because of space limitations, it was outside the detector array and subtended a rather small angle at the collector foil. Spectra were also collected with the additional requirement of a $\beta$ coincidence. The resulting quadruple coincidence spectrum for strip 4 of each double sided strip detector is shown in Fig. 43. No kinematic corrections have been applied to this spectrum. The additional requirement of a $\beta$ coincidence considerably reduces the accidental background even without the kinematic correction.

The detection of 14,000 triple-coincidence decay events at 0.15% coincidence efficiency into the 9.59 MeV state of $^{16}$O corresponds to approximately $2 \times 10^{-6}$ of the total observed $^{17}$Ne decays. This is about a factor of $10^4$ more than the number of $\beta$-delayed proton decays through the IAS estimated to populate the tail of the 7.117 MeV state in $^{16}$O and to have been detected in this experiment. While it would be straightforward with the $^{17}$Ne yields recently achieved with TISOL ($\geq 2\times10^5$ s$^{-1}\mu$A$^{-1}$), with improved angular resolution, and with much larger solid angle coverage, to achieve the count rate required to detect the tail of this sub-threshold state in $^{16}$O, further detector improvements have to be made to suppress false triple coincidences resulting primarily from coincidences with $\beta$-particles.

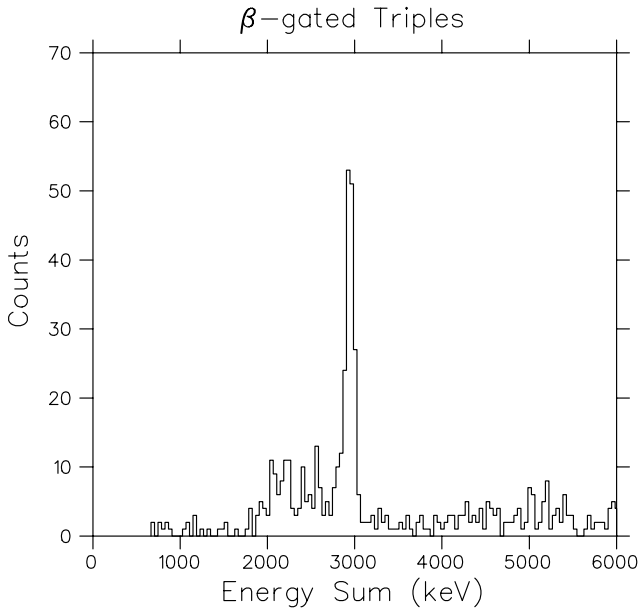


Fig. 43. Triple coincidence energy-sum spectra for a single strip (strip 4) of each double-sided strip detector with the additional requirement of a $\beta$-coincidence.

In the next phase of our study, with improved $\beta$ suppression and much better statistical accuracy, it should be feasible to determine the influence of the tail of the sub-threshold 7.117 MeV state on the $\alpha$-spectrum from the decay of the IAS into the 9.59 MeV state of $^{16}$O. This will provide an independent determination of the effect of this sub-threshold state on the $^{12}\mathrm{C}(\alpha,\gamma)^{16}\mathrm{O}$ cross section for comparison with the result obtained from $^{16}$N decay in Expt. 589.

**Experiment 744**
**A kinematically complete study of $\pi^- p \rightarrow e^+ e^- n$**
*(M.A. Kovash, Kentucky)*

At sufficiently low pion momentum the electroproduction of pions from the nucleon, and the inverse process, radiative pair production, $\pi^- p \rightarrow e^+ e^- n$, are reactions that are completely dominated by the absorption of electric dipole photons and the production of $s$-wave pions through the seagull diagram. As a result, these processes can be used to probe the axial response of the nucleon in a relatively model-independent way. While this has been attempted experimentally for a number of years in studies of $\pi^-$ electroproduction from the neutron, there have been serious difficulties associated with the use of a deuterium target, as well as the problem of reaching sufficiently low values of pion momenta. At TRIUMF we have initiated a study of radiative pair production using the $3\pi$ acceptance RMC detector. Our goal is to make a complete kinematic study of this reaction and extract the nucleon axial radius.

As implemented at TRIUMF, radiative pair production offers several significant advantages over previous electroproduction work: the target will be pure hydrogen with little contamination; the pion beam momentum will be set low, where the reaction dynamics are well understood; and the large detector acceptance will enable a Rosenbluth separation into transverse, longitudinal and interference structure functions.

To date, we have completed two test runs using $CH_2$ targets in the RMC detector. The goals of these runs have been to learn the methods and optimize the techniques for separating $e^+e-$ pairs from the prolific real and accidental coincidence backgrounds. To this end we have made extensive studies, both with Monte Carlo simulations as well as with real data, of the response of the RMC trigger scintillators and tracking wire chambers to real and background events. These studies have uncovered some deficiencies which can readily be improved before production data are collected, primarily through the use of improved time-of-flight measurements between the beam scintillators and the outer D counters of the RMC scintillator stack. With improved TOF, and using corrected $\Delta E$ information from the scintillators, background pions and protons can be virtually eliminated.

It is expected that continued analysis of the present test run data will provide a first, low-statistics measurement of the axial form factor. In addition, work has begun at the Univ. of Kentucky on a new liquid hydrogen target needed for future high-statistics production running.

**Experiment 767**
**Direct measurement of sticking in muon catalyzed $d-t$ fusion**
*(M.C. Fujiwara, UBC; P. Kammel, U.C. Berkeley/ LBL; G.M. Marshall, TRIUMF)*

Muon catalyzed fusion ($\mu$CF), a phenomenon which connects many disciplines of physics including particle, nuclear, atomic, molecular and condensed matter, is the subject of a substantial body of fundamental and applied research. Although there has been much interest in possible applications, such as the old dream of energy production and the recently proposed intense source of fast neutrons or slow muons, the processes of $\mu$CF have also provided one of the most precise testing grounds for the fundamental theory of few-body interactions.

Sticking, in which the muon is attached to a helium nucleus after fusion, is one of the most important parameters in $\mu$CF, because it limits the number of fusions that one muon can catalyze. Despite a great amount of effort, the discrepancies between theory and experiment and among different experimental groups still persist. The experimental sticking values

have been consistently and substantially smaller than theoretical predictions.

Calculations of sticking are challenging, due to an interplay of the Coulomb and strong interactions in highly non-adiabatic few-body systems, yet theoretical predictions have now converged to agree within a few percent. They cannot, however, be readily compared to experiment because most experiments are primarily sensitive to *final sticking*, which is a combination of the intrinsic *initial sticking* and *stripping*, or collisional reactivation of the muon from $\mu\alpha$ in the target medium. Recent developments in the theoretical treatment which go beyond the sudden approximation further exacerbated the discrepancy, and it is now claimed that there is little room for improvement in calculation of both initial sticking and stripping within the current theoretical framework. New experimental insight is therefore important and timely.

The confusing history of experimental sticking results is thought to be partly due to the problems associated with the conventional neutron method, on which the majority of world data is based. A recent PSI experiment [Petitjean *et al.*, Hyp. Int. **82**, 273 (1993)] at medium density has shown that detection of $\mu\alpha$ and $\alpha$ gives the most direct measurement of sticking, yet the results are still about $2\sigma$ smaller than theory. At high densities, no direct $\mu\alpha/\alpha$ measurements are available, and the indirect neutron method, supposedly most sensitive at these densities, gives values about $3\sigma$ smaller than theory.

In this experiment, we hope to achieve the following tasks; (1) a model independent separation of initial sticking and stripping, and (2) a direct $\mu\alpha/\alpha$ ratio measurement of sticking at high density. We will address these crucial issues with a new method, which takes advantage of the hetero-structure nature of thin hydrogen film targets as developed for Expt. 613, together with neutron and silicon detectors in a $\mu\alpha$–$n$ coincidence measurement. The proposed experiment will provide the long-awaited experimental determination of initial sticking with only a small stripping correction, where the stripping process itself can be separately studied for the first time. It will also enable the first direct $\mu\alpha$–$n$ coincidence measurement in a high density environment, where the discrepancy between experiment and theory is largest. We intend to measure initial sticking to 5%, comparable to theoretical uncertainties, hence providing an unambiguous test of the theory of sticking.

Preliminary measurements as well as extensive Monte Carlo studies have been performed, and we plan to start data-taking in 1998. The details of the new method are discussed in Fujiwara *et al.* [Hyp. Int. **101/102**, 613 (1996)].

**Experiment 778**
**$\pi^{\pm}p$ differential cross sections in the Coulomb-nuclear interference region**
*(G.R. Smith, TRIUMF; R. Meier, Tübingen; P. Camerini, Trieste; M.E. Sevior, Melbourne)*

This experiment was presented to the TRIUMF EEC in July, 1996 and was awarded high priority. Development shifts for the experiment took place in the fall of 1997 and the experiment will begin data acquisition in the spring of 1998. A scintillation counter stack is being designed and will be constructed for this experiment by our Univ. of Trieste and Univ. of Tübingen collaborators. In addition, a supercooled planar liquid hydrogen target is being developed at TRIUMF for this experiment and will be employed in conjunction with the CHAOS spectrometer in the TRIUMF M13 beam line.

The primary goals of the CHAOS physics program to date have been to test predictions and measure parameters of chiral perturbation theory. To this end, we have performed measurements in the $\pi^{\pm}p$ sector of pion induced pion production (Expt. 624) and elastic analyzing powers (Expt. 560). Experiment 778 deals with the next stage of this program, namely the measurement of $\pi^{\pm}p$ absolute differential cross sections in the very forward angle region where Coulomb scattering interferes destructively (constructively) with $\pi^{+}p$ ($\pi^{-}p$) hadronic scattering amplitudes.

The experimental goals of the proposed measurements are to provide absolute differential cross sections to a precision of $\leq$5% for both $\pi^{\pm}p$ elastic scattering at angles greater than 5°, for pion bombarding energies between 20 and 70 MeV.

The physics goals are to use these data to provide information missing in the current partial wave analyses on the real part of the isospin-even forward scattering amplitude. The real part of the isospin even amplitude $D^{+}$ at $t$=0 will be measured in this experiment to a precision of a few percent. This will greatly improve the determination of $\pi N$ scattering amplitudes, and as a result would improve the determination of the $\pi N$ coupling constant and $\pi N$ scattering lengths, in addition to the $\pi N$ $\Sigma$ term, all observables of crucial importance. In addition, the proposed measurements are important in the context of understanding isospin breaking due to the $u-d$ quark mass difference.

The above goals alone provide sufficient justification for this experiment. However, in the proposal we showed, in addition to providing Re($D^{+}$) at $t$=0 for partial wave analysis (PWA) improvements, how a systematic set of measurements in the Coulomb-nuclear interference (CNI) region can be used to measure the isospin even, $s$-wave scattering length $a^{+}_{0^{+}}$ and the isospin even $P$-wave scattering length $a^{+}_{1^{+}}$ *directly.* This

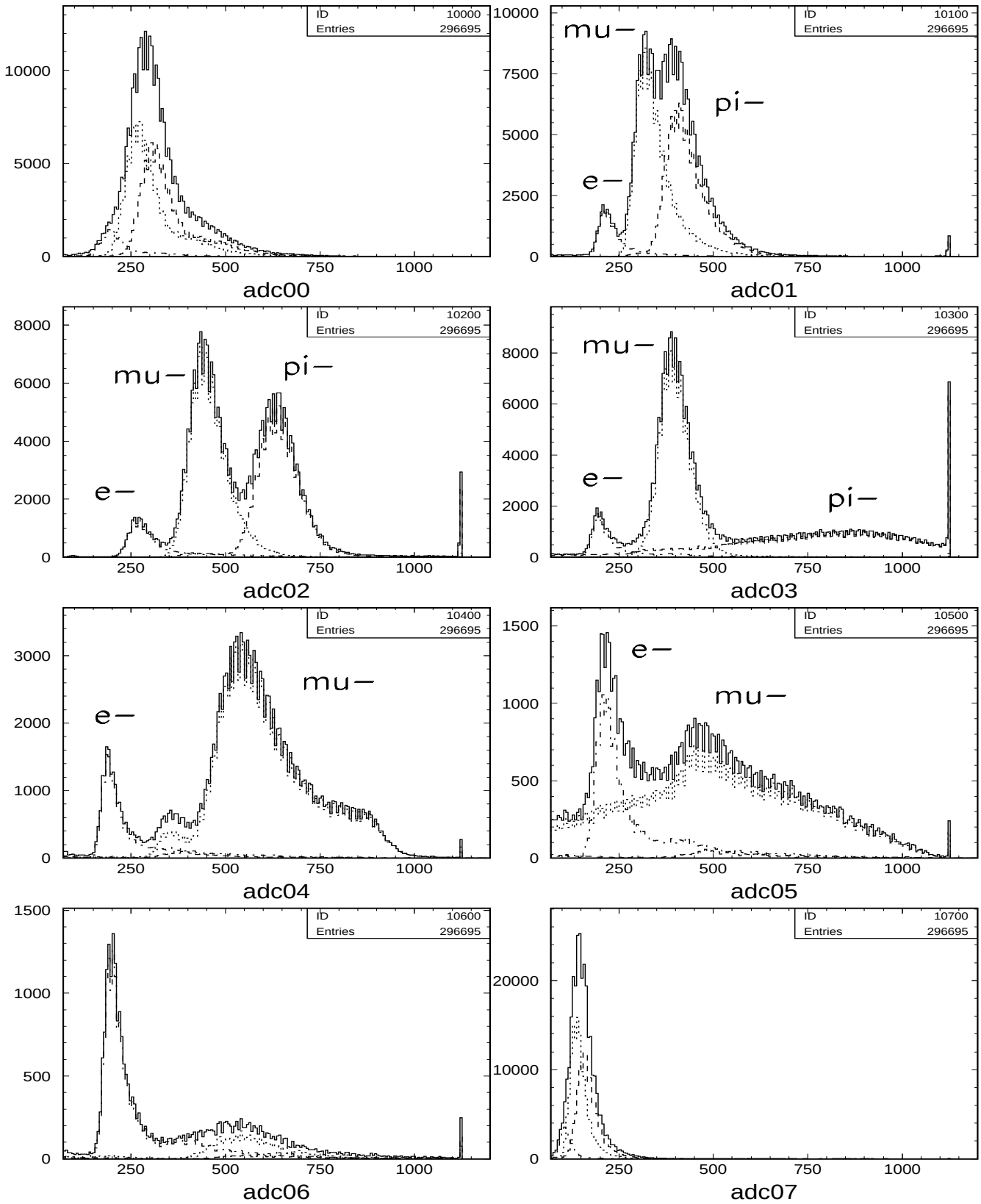


Fig. 44. Pulse height spectra obtained with the prototype $\pi/\mu$ PID scintillator stack. The contributions from each particle species, as determined independently from S0-S7 TOF, are plotted separately and labelled in each figure. The total is also shown. These data were acquired for 125 MeV/c, negative channel polarity.

new, direct information can then be used for an independent determination of the $\pi N$ $\Sigma$ term. The $\Sigma$ term is of fundamental importance, it is a direct measure of chiral symmetry breaking, and can be used to provide a measure of the strange sea quark content of the proton. The CNI measurements proposed here can be used to measure $\Sigma_{\pi N}$ in a manner less dependent on the results of PWA.

The proposal may be viewed in colour using the Web, at http://www.triumf.ca/chaos/cni.ps.

This year the effort on this experiment focused on Monte Carlo simulations, design specifications for the cryogenic target, development of partial wave analysis tools, and the testing of a prototype $\pi/\mu$ stack.

The fall, 1997 development shifts were used to test a prototype scintillation counter stack needed for $\pi/\mu$ particle identification in this experiment. A scintillator (S0) was placed 1.5 m upstream of the stack in this test to simulate the information provided by the CHAOS incident beam trigger counter. The stack itself consisted of six scintillation counters, each roughly 20 $\times$ 20 cm$^2$ and 13 mm thick. S1 was half this area and thickness, S6 was the same area but half the thickness. Aluminum absorbers were placed between each scintillation counter such that pions would stop in counter i and muons would stop in counter i+2. 18 incident pion momenta between 65 and 150 MeV/c were studied in the M13 channel with this prototype. The absorber thicknesses were adjusted for each beam momentum. In addition, studies were made with fixed absorber thicknesses at several momenta. Positive PID necessary to test the capability of the stack was obtained using both rf referenced TOF down the M13 channel to the stack, as well as using the TOF between a scintillator (S7) placed just outside the last element of the beam line, and S0 which was a further 4.2 m downstream. The information gathered was useful both to check the proposed PID algorithm as well as to train the neural network used in the analysis.

Typical pulse height spectra obtained at an incident momentum of 125 MeV/c ($\pi^-$) are shown in Fig. 44. The various particle species ($\pi$, $\mu$, $e$) are differentiated using different line types in this figure by making use of the S0–S7 TOF. In this way the ability of the stack to mass identify particles based solely on the pulse height information can be ascertained. The large pulse heights associated with stopping pions (muons) are evident in S3 (S5). The particle identification efficiency obtained from the product of all the available information is provided by the neural network. The results are presently being analyzed and will be used to fine tune the stack design with the goal of having the final stacks in place by spring 1998.

**Experiment 781**
**Investigations of the $\pi\pi$ invariant mass distributions of nuclear $(\pi^+, \pi^-\pi^+)$ reactions with the CHAOS detector**
*(M. Sevior, Melbourne)*

Experiment 781 is a continuation of CHAOS Expt. 653. In this experiment we measured 4-fold differential cross sections at incident pion energy 280 MeV for the reactions:
$^2$H$(\pi^+, \pi^+\pi^-)X$ and $^2$H$(\pi^+, \pi^+\pi^+)X$,
$^{12}$C$(\pi^+, \pi^+\pi^-)X$ and $^{12}$C$(\pi^+, \pi^+\pi^+)X$,
$^{40}$Ca$(\pi^+, \pi^+\pi^-)X$ and $^{40}$Ca$(\pi^+, \pi^+\pi^+)X$, and
$^{208}$Pb$(\pi^+, \pi^+\pi^-)X$ and $^{208}$Pb$(\pi^+, \pi^+\pi^+)X$.

We found a marked enhancement just above threshold for the isospin 0 channel $\pi^+\pi^-$ on carbon, calcium and lead compared to deuterium. No such enhancement was present in the $\pi^+\pi^+$ isospin 2 channel for the reaction on any nucleus [Bonutti *et al.*, Phys. Rev. Lett. **77**, 603 (1996)].

We do not understand the origin of this enhancement. It could be due to:

1. An enhancement of the one pion exchange diagram in a nuclear medium
2. The existence of a new 2 nucleon reaction mechanism for pion induced pion production
3. A final state interaction between the outgoing pions due to a greatly increased attraction between the $\pi^+\pi^-$ within the nuclear medium.

Since the interaction between pions is governed by the properties of the QCD vacuum state, explanations (1) and (3) may imply that QCD has a vastly different vacuum structure within the nuclear medium. Explanation (2) would require some interesting new reaction dynamics.

The 1996 summer EEC committee awarded this experiment 20 shifts of high intensity running at medium priority to investigate the energy dependence of the effect. We completed the data-taking phase of the experiment in August, 1997. We ran on a $CD_2$ target at 280 MeV and on a $^{45}$Sc target at incident $\pi^+$ energies of 320, 300, 280, 260 and 240 MeV. The 240 MeV data was acquired during a polarized beam period. The TRIUMF high intensity source was used to provide 7 $\mu$A of beam down beam line 1A. Since 240 MeV is near the peak of the pion production curve and adequate flux of pions was available even at at this low primary proton intensity.

Figure 45 shows very preliminary histograms of the invariant mass distributions from the $^{45}$Sc$(\pi^+, \pi^+\pi^-)X$ and $CD_2(\pi^+, \pi^+\pi^-)X$ reactions at energies of 320, 300, 280 and 260 MeV. Data for 240 MeV have not yet been skimmed and so are not shown

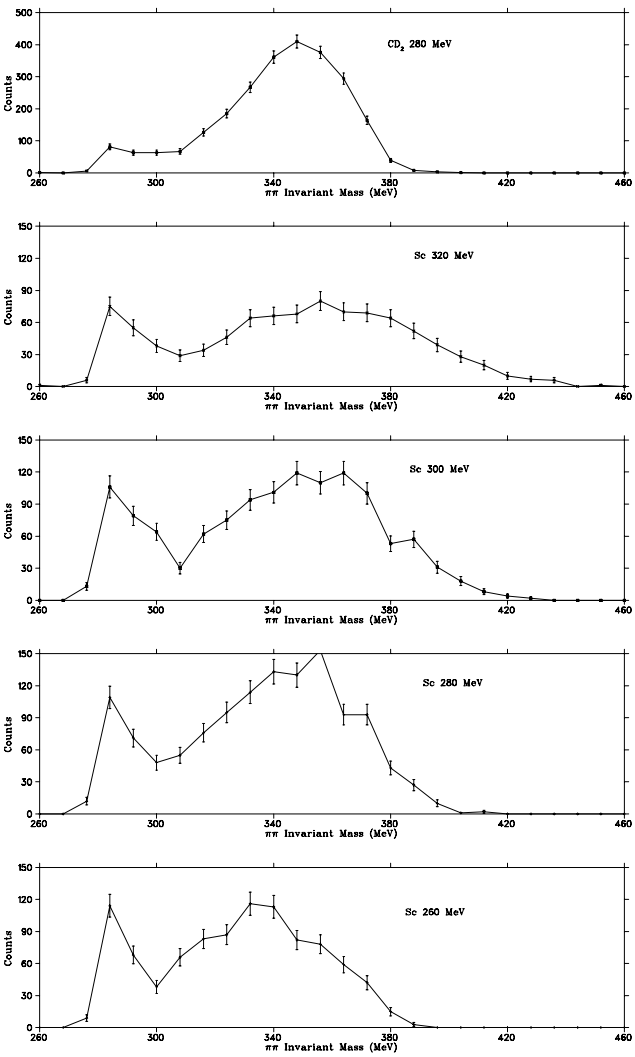


Fig. 45. Preliminary histograms of the $\pi - \pi$ invariant mass distributions.

in this report. No acceptance corrections of any type have been made and only crude particle identification is in place. Nevertheless it is clear that the region below 300 MeV provides far less of the yield from the $CD_2$ target than the $^{45}$Sc target. Moreover, the enhancement in yield below 300 MeV is present at all energies.

We plan to complete the data analysis at the Univ. of Melbourne and TRIUMF in 1998.

**Experiment 785**
**Pion double charge exchange on $^3$He with CHAOS**
*(R. Tacik, TRIUMF/Regina)*

This experiment was run in M11 in the summer. It involved the measurement of both the inclusive $^3\mathrm{He}(\pi^-, \pi^+)$ and semi-exclusive $^3\mathrm{He}(\pi^-, \pi^+ n)$ double charge exchange (DCX) reaction channels, at incident pion energies below 100 MeV. It is complementary to earlier experiments 719 and 725, which are currently being analyzed by the CHAOS collaboration.

One particularly novel feature of Expt. 785 was that it involved the simultaneous operation of CHAOS and an external neutron detector array. A schematic scale view of the set-up, with the neutron array in one of the two positions used during the measurements, is provided in Fig. 46. The hardware coincidence between the neutron array and CHAOS was made at the CHAOS second level trigger stage. Calibration data for the neutron array was obtained using charged particles from the incident and scattered beams, and cosmic rays, as well as from the $^3\mathrm{He}(\pi^-, dn)$ reaction, where the deuteron was detected in CHAOS. Experiment 785 employed the same basic Regina/TRIUMF liquid helium target as had been previously used for Expt. 725, but modified for L$^3$He instead of L$^4$He. The target operated flawlessly for the entire run.

The general aim of Expt. 785 was to obtain high quality DCX data for $^3$He with which to confront all models of the DCX process. No other measurements have been performed below $T_\pi = 120$ MeV. A more specific aim of Expt. 785 was to search for the existence of a narrow resonance in the $\pi NN$ subsystem, called the $d'$. The effect of the $d'$ has been proposed as the explanation for the otherwise unexplained behaviour of the total DCX cross sections near $T_\pi = 50$ MeV, as measured on virtually all heavier nuclear targets which have been studied. Use of the helium isotopes as targets provides the best potential for separating the influences of nuclear structure and the underlying DCX reaction mechanism.

A relatively small part of the Expt. 785 running time was spent on the inclusive $^3\mathrm{He}(\pi^-, \pi^+)$ reaction. Measurements were taken at several incident pion energies between 70 and 100 MeV. The analysis of this part of the experiment forms part of the Ph.D. thesis project of Mr. J. Graeter from the Univ. of Tübingen. The on-line results showed that the total DCX cross section in $^3$He does not drop as quickly with energy as expected from conventional calculations.

Most of the Expt. 785 running time was spent on accumulating statistics in the neutron time-of-flight

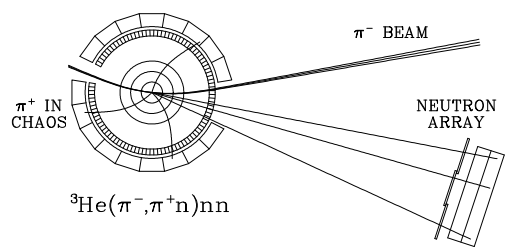


Fig. 46. Schematic scale view of the Expt. 785 experimental set-up.

spectra for the semi-exclusive $^3$He$(\pi^-, \pi^+ n)$ reaction. The analysis of this part of the experiment constitutes the Ph.D. thesis project of Mr. G. Tagliente from UBC. Measurements were taken at $T_\pi$ = 65 and 75 MeV. The total DCX cross section is larger at the higher energy, but the signal from a $d'$ was predicted to be larger at the lower energy. Within the $d'$ model, the reaction proceeds mostly via the two-step process: $\pi^-$ $^3$He $\rightarrow d'n \rightarrow (\pi^+ nn)n$. The detection of the $\pi^+$ in CHAOS serves as the signature of DCX. Because of the two-body intermediate state, the existence of the $d'$ should manifest itself as a narrow peak in the neutron energy spectrum measured at a particular angle, above a combinatorial background arising from the detection of one of the neutrons from $d'$ decay, rather than the one which recoiled against it in the intermediate state. Model calculations predict a smooth energy dependence for this background. The same holds true for neutrons produced via conventional mechanisms. On-line results did not show a sharp peak in the measured neutron energy distributions. However, final conclusions cannot be made until the data analysis is completed. There was a large experimental background associated with electrons in the beam which must be dealt with properly, and more detailed comparisons with model simulations must be performed.

**Experiment 793**
**Production of an intense $^{15}$O beam**
*(J. D'Auria, TRIUMF)*

An important project planned for the new ISAC accelerated radioactive beam facility is a measurement of the rate of the $^{15}$O$(\alpha, \gamma)^{19}$Ne reaction, which is believed to be the main breakout reaction for the hot CNO cycle. This is believed to play an important role in such cataclysmic events as novae and production of x-ray bursts in the universe, leading to the production of heavy elements. At ISAC, this reaction will be studied in inverse kinematics using an accelerated beam of the short-lived isotope, $^{15}$O(2.1 m), with a gaseous target of helium. Due to the low resonance strength of the reaction, a beam of the order of $10^{10}$ s$^{-1}$ or higher will be required to properly perform this study. Unfortunately, such an intense beam has never been observed from an on-line isotope separator due to the reactivity of the oxygen atom, and the purpose of Expt. 793 is to develop an approach that can be used to produce such an intense beam.

There are two approaches that have been proposed to produce such an intense beam at ISAC. The first method involves the use of a thick target of the appropriate material which will release the oxygen species, coupled with the appropriate ion source to produce the required ion beam. The second approach is to use a low energy ($\lesssim$ 30 MeV) proton beam with a gaseous low $Z$ target, transferring the produced volatile oxygen species to an ion source, leading to the required ion beam. The latter approach in fact has proven to be very successful to produce high quantities of $^{15}$O for nuclear medicine applications, however, the coupling to the ion source requires considerable development. This approach will be pursued separately. Experiment 793 will explore the former approach and initial studies were performed in 1997 using the TISOL facility.

Three beam periods (3 shifts each) were used to initiate this study. A special quartz target oven and transfer tube were constructed and installed to hold the target material. This allows the reactive, volatile oxygen species to be delivered efficiently to the plasma tube of the ECR source. It should be noted that oxygen beams had only been observed previously at TISOL with graphite ovens.

Using targets of zeolite and, separately, a $MgF_2$/graphite mixture, beams of $^{14,15}$O were observed but in intensities much lower than desired. Several experimental problems contributed to the poor results. Some of the studies will be repeated along with further studies of a variety of other target materials.

**UBC undergraduate course beam time**
*(S. Yen, TRIUMF)*

In November, 9 shifts of beam time were used on M13 as part of the laboratory part of the UBC undergraduate nuclear physics courses Physics 473 and 414. Students had previous experience in the lab with gamma ray detectors; this exercise was designed to allow them to measure some real physical quantities using particle beams from an accelerator. Students came to TRIUMF in groups of 5 at a time, for about 3 hours each. In this time, they were asked to measure the mass of the muon, and the half-life of $^{11}$C.

To keep things as simple and robust as possible, the detector consisted of two scintillators in the beam line, such that 55 MeV/c pions would stop in the first scintillator and muons of that momentum would stop in the second scintillator. The students were asked to step the channel momentum in steps of 5 MeV/c and observe the shift in time of the rf pulse relative to the signal in the scintillators on an oscilloscope. The change in time as a function of momentum allowed them to determine the muon mass.

In the second part of the lab, a 6 mm thick piece of polyethylene was irradiated in a beam of 125 MeV/c pions for about 30 minutes (during which time the students were taken on a walk-around tour of TRIUMF). The positron activity of sample as a function of time was then measured in a NaI gamma ray detector, in order to determine the half-life of $^{11}$C.